

UNCLASSIFIED

AD NUMBER

ADA286600

CLASSIFICATION CHANGES

TO: unclassified

FROM: confidential

LIMITATION CHANGES

TO:

Approved for public release, distribution unlimited

FROM:

Distribution authorized to DoD only; Administrative/Operational Use; 29 APR 1969. Other requests shall be referred to US Defense Nuclear Agency, 6801 Telegraph Road, Alexandria, VA 22310-3398. Pre-dates formal DoD distribution statements. Treat as DoD only.

AUTHORITY

30 Apr 1981 DoDD 5200.10; DNA ltr 23 Aug 1994

THIS PAGE IS UNCLASSIFIED

AD-A286 600



POR-3021  
(WT-3021)

①

# FERRIS WHEEL SERIES

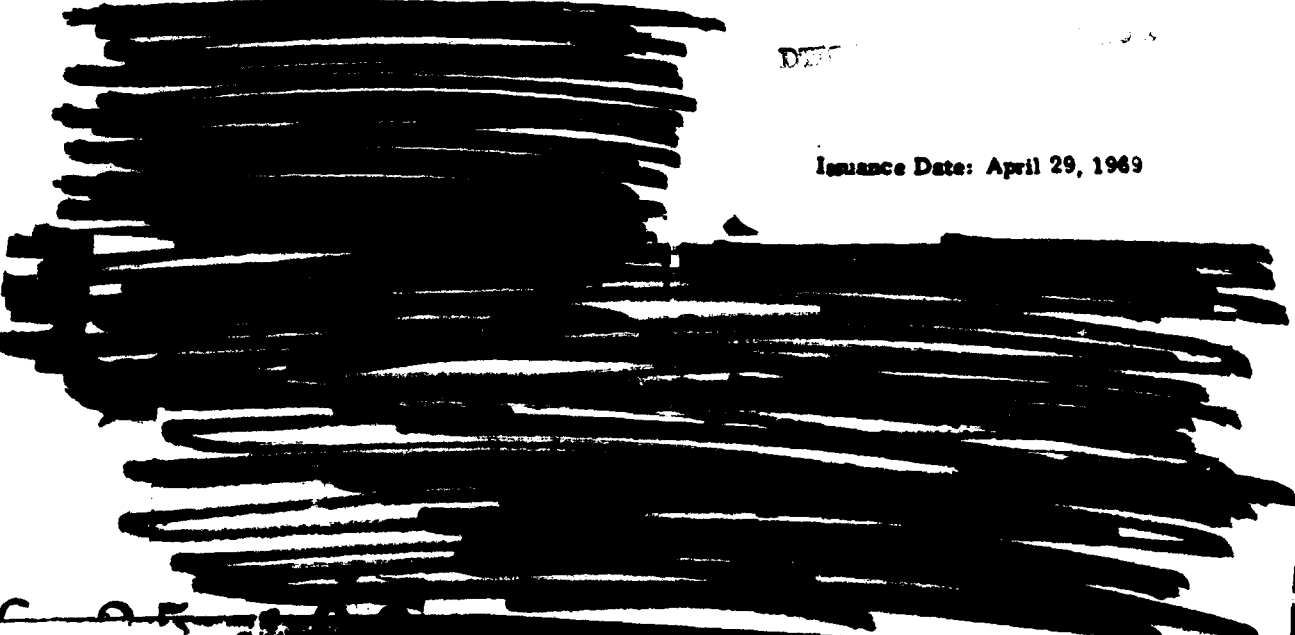
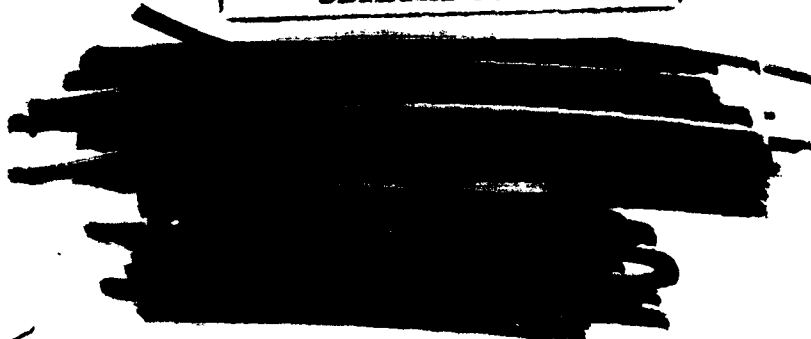
## SHOT TINY TOT

### TECHNICAL DIRECTOR'S SUMMARY REPORT

DISTRIBUTION STATEMENT A

Approved for public release  
Distribution Unlimited

DTIC  
ELECTE  
AUG 26, 1990  
S B D



Issuance Date: April 29, 1969

94-27396



76B



Defense Nuclear Agency  
6801 Telegraph Road  
Alexandria, Virginia 22310-3398

IMTS

23 August 1994

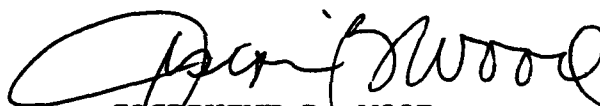
MEMORANDUM FOR DEFENSE TECHNICAL INFORMATION CENTER  
ATTENTION: DTIC/OCC

SUBJECT: Documents Submitted for Inclusion In the DTIC System

The Defense Nuclear Agency Information Management Technical Support Office requests the enclosed technical reports be included in the DTIC system.

Distribution statement 'A' (approved for public release) applies. Please direct all inquires to Mrs. Naomi E. Fields at (703) 325-1038.

FOR THE DIRECTOR:

  
JOSEPHINE B. WOOD  
Chief, Technical Support

Enclosures

POR-6206 (2)  
POR-3021 (2)  
POR-6546 (2)  
POR-2039 (2)  
POR-6300 (2)  
POR-2725 (2)  
POR-6337 (2)  
POR-3000 (2)  
WT-561 (2)  
WT-601 (2)

*[Handwritten scribble]*

POR-3021 *Final*  
(WT-3021)

FERRIS WHEEL SERIES

SHOT TINY TOT

TECHNICAL DIRECTOR'S SUMMARY REPORT

Accession For	
NTIS GRA&I	<input checked="" type="checkbox"/>
DTIC TAB	<input type="checkbox"/>
Unannounced	<input type="checkbox"/>
Justification	
By	
Distribution	
Availability Codes	
Dist	Avail and/or Special
<i>[Handwritten mark]</i>	

M. L. Merritt, Scientific Director

Sandia Laboratory, Box 5800  
Albuquerque, New Mexico 87115

*[Redacted box]*

This document is the author(s) report to the Director, Defense Atomic Support Agency, of the results of experimentation sponsored by that agency during nuclear weapons effects testing. Accordingly, reference to this material must credit the author(s). This report is the property of the Department of Defense and, as such, may be reclassified or withdrawn from circulation as appropriate by the Defense Atomic Support Agency.

*[Large handwritten scribble]*

[REDACTED]

ABSTRACT

**[REDACTED]** Tiny Tot was a **[REDACTED]** nuclear burst on the flat surface of a large underground cavity in granite. It was fired to produce data for empirical extrapolation and to normalize theoretical (computational) prediction of ground shock from surface bursts on hard rock, as well as for hard-rock crater data.

**[REDACTED]** Ground-motion experiments showed a coupling factor of **[REDACTED]** percent at the 1-kilobar level. The true crater formed was 14 feet in radius and **[REDACTED]** feet deep, considerably smaller than it would have been in soils where most other data have been obtained. Air-pressure measurements included one at 66,000 psi, the highest yet by nonphotographic methods; they also seem to show pronounced degradation of the airblast from the so-called flat surface. The stemming and containment plan was satisfactory, with only a slight leak of radioactive xenon and iodine.

**[REDACTED]** The associated calculations were verified to better than a factor of two so far as peaks are concerned, as good as could be expected. Waveforms were short in duration relative to the data, raising questions about the relaxation adiabats implied by the equation of state used.

**[REDACTED]** Extrapolation of the data beyond the low kilotons is not valid; extrapolation of calculational methods probably is valid provided allowances are made for effects not observed at Tiny Tot's low yield.

DNA  
(b)(3)  
(4)(c)



CONTENTS

ABSTRACT ----- 5

CHAPTER 1 INTRODUCTION ----- 11

    1.1 Objectives----- 13

    1.2 Test Configuration ----- 14

    1.3 Experiment Plan ----- 16

CHAPTER 2 GROUND SHOCK ----- 20

    2.1 Instrumentation ----- 20

    2.2 Experiment Design ----- 22

    2.3 Cavity Condition----- 24

    2.4 Results ----- 25

        2.4.1 Results, Times of Arrival ----- 25

        2.4.2 Results, Peak Stresses and Velocities ----- 25

        2.4.3 Results, Precursors and Other Thoughts ----- 27

    2.5 Instrument Performance ----- 30

    2.6 Empirical Summary ----- 30

CHAPTER 3 CALCULATIONS ----- 48

    3.1 Granite Equation of State ----- 49

    3.2 Calculation for a Contained Burst ----- 51

    3.3 Calculational Results, Peaks ----- 51

    3.4 Calculational Results, Waveforms ----- 55

    3.5 Calculational Results, Surface Motion ----- 58

    3.6 Calculational Results, Extrapolations ----- 60

    3.7 Summary of Ground-Motion Experiment as Clarified by the  
        Calculation ----- 62

CHAPTER 4 CRATERING ----- 86

    4.1 Introduction ----- 86

    4.2 Crater Dimensions ----- 86

    4.3 Comparison with Other Data ----- 89

CHAPTER 5 AIR PRESSURES ----- 100

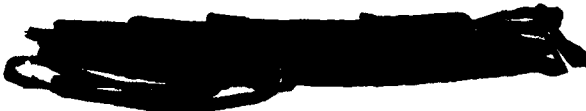
CHAPTER 6 THE CAVITY ----- 109

    6.1 Cavity Design ----- 109

    6.2 Stemming Design ----- 110

    6.3 Shot Time Behavior ----- 112

    6.4 Reentry Observations ----- 113



6.5 Condition of the Cavity	113
6.6 Conclusions	114
<b>CHAPTER 7 SURFACE AND SEISMIC MOTIONS</b>	<b>118</b>
7.1 Surface Motions	118
7.2 Seismic Decoupling	119
<b>REFERENCES</b>	<b>123</b>

**TABLES**

1.1 List of Tiny Tot Projects	18
1.2 Time Scale, Tiny Tot	18
2.1 Index of Main Gage Holes	32
2.2 Velocity and Displacement Data	32
2.3 Acceleration Data	33
2.4 High Stress Data	34
2.5 Slifer Cable and Quartz Gage Data	34
2.6 Data from Other Shots in Granite	35
2.7 Instrument Performance	36
3.1 Granite Equation of State	63
3.2 Positions of Waveform Comparisons	63
4.1 Tiny Tot and Other Crater Data	91
5.1 Air Pressure Measurements	105
6.1 RAMS Unit Locations	115
7.1 Project 1.2 Surface Motion Data	120
7.2 USCGS Surface Motion Data	120

**FIGURES**

1.1 Plan and elevations of Tiny Tot excavations	19
2.1 Gage and granite block installation at Tiny Tot working point	37
2.2 a and b Hugoniot data of granite and grout	38
2.3 Tiny Tot device in place	40
2.4 View upward of flat surface toward working point	40
2.5 View of lower left-hand quadrant of flat surface, illustrating steel net and spacing of rock bolts	41
2.6 Region around the working point during installation of gages, illustrating the extent area was cleared of netting	41
2.7 Measured times of arrival versus distance	42
2.8 Measured peak stresses versus distance	43
2.9 Measured peak velocities versus distance	44
2.10 Precursor and peak stresses compared	45
2.11 Precursor waveforms from SRI gages	47
2.12 Waveforms from HTRI gages	47
3.1 Hugoniot implied by the equation of state used in the calculation	64
3.2 Hugoniot implied by the equation of state compared to Hugoniot data	65
3.3 Calculated peak stress compared with data	66

~~CONFIDENTIAL~~

3.4	Calculated peak velocities compared with data	67
3.5	Calculated arrival times compared with data	68
3.6	Calculated peak stress contours	69
3.7	Calculated peak velocity contours	70
3.8	Velocity field at the end of the calculation	71
3.9	Peak velocity contours, as calculated and by Cooper's fit	72
3.10	Waveform comparisons, Gage 103 PK	73
3.11	Waveform comparisons, Gage 303 PL	74
3.12	Waveform comparisons, Gage 305 PL	75
3.13	Waveform comparisons, Gage 207 UR	76
3.14	Waveform comparisons, Gage 208 UR	77
3.15	Waveform comparisons, Gage 209 UR	78
3.16	Waveform comparisons, Gage 210 UR	79
3.17	Calculated contours of arrival times of peaks	80
3.18	Calculated velocity versus time at 3 meters near surface	81
3.19	Calculated velocity versus time at 5 meters near surface	82
3.20	Calculated velocity versus time at 7.1 meters near surface	83
3.21	Calculated velocity versus time at 10 meters near surface	84
3.22	Comparison of Tiny Tot and a 1.5-megaton calculation, both scaled to 1 megaton	85
4.1	Topography of the cavity face before the shot	92
4.2	Topography of the cavity face after the shot	93
4.3	Crater topography	94
4.4	Side view of Tiny Tot crater	95
4.5	Front view of Tiny Tot crater	96
4.6	Front view of Tiny Tot crater	97
4.7	Comparison of Tiny Tot crater radius with radii from other near-surface bursts	98
4.8	Comparison of Tiny Tot crater depth with radii from other near-surface bursts	99
5.1	Arrival times of air shock	100
5.2	Peak air pressure versus distance	107
5.3	Waveforms of air pressure at Station 4	108
6.1	Radiation intensity versus time measured by RAMS units at various positions in the stemming	110
6.2	Detail of cavity wall after the shot	117
7.1	Comparison of SRI (Project 1.2) and USCGS surface-motion data	121
7.2	Azimuthal variation of peak surface acceleration	122

[REDACTED]

## CHAPTER 1

### INTRODUCTION

[REDACTED] Tiny Tot was a [REDACTED] nuclear shot fired on the flat face of a cavity mined in granite. It was part of the DASA Ground Shock and Cratering Program, officially nicknamed Ferris Wheel. The guiding principle of Ferris Wheel was to develop an adequate prediction technique, based primarily on theory and computer calculations but directly supported by definitive field experiments. In this program, the nuclear-effect test was to play the role of a laboratory experiment to verify theory, not an empirical entity to be explained a posteriori.

DNA  
(b)(3)  
(4)(1)

[REDACTED] As originally conceived (Reference 6), the Ferris Wheel experimental program was to be entirely nuclear, consisting of experiments to investigate the effects on ground shock and cratering, of depth of burst, of early energy leakage by radiation transport (the Brode effect), and, to a limited extent, of yield and of medium properties. The experiments were to be carried out at the lowest yield possible in order to conform with national limitations then in force on the yield of aboveground nuclear detonations.

[REDACTED] Ferris Wheel's initial or B-series shots were to be very small surface shots in playa, but this initial series was never executed. In May 1963 a significant part of the instrumentation for two small nuclear shots and one accompanying HE detonation

[REDACTED]

[REDACTED]

had been completed; in fact, the HE experiment was to be fired within 3 days. A preshot announcement created an unfortunate reaction prejudicial to the negotiations leading up to the present limited-test-ban treaty, and the series was called off by order of the President.

[REDACTED] With the need for data on ground motion beneath large detonations still a requirement, alternative experiments were considered to give partial answers. Air Vent was a series of HE detonations to study closely surface-burst scaling and to compare crater depth-of-burst curves for the playa of Area 5 with areas of previous experience. Two 20-ton HE detonations known as Flat Top took advantage of the instrumentation installed for the initial B-series to examine the ground motions themselves; Flat Top also included a shot on limestone with similar instrumentation (Reference 7).

[REDACTED] In the meantime pressure had arisen for direct information about the ground-shock effects of nuclear surface bursts on hard rock (Reference 8). It was concern over underground protective structures such as deep command centers that originally gave rise to Ferris Wheel and caused its A-2 shot to be put near the top of the priority list. (By mid-1967 the concern was over the proposed Advanced Ballistic Missile System, but the questions remained much the same.) A test concept was drawn up in June 1963 for A-2 as a 500-ton shot on the basalt of Buckboard Mesa in Area 18 of the Nevada Test Site (Reference 9).

[REDACTED] With the Test Ban Treaty and the certainty that surface shots would not be permitted for the foreseeable future, a revised test concept was submitted in February 1964 for conducting a simulated surface burst within a large underground cavity

[REDACTED]

(References 10, 11). Since the accepted concept of superhard protective construction requires a site of hard rock (generally granite) and since the surface-burst experiment was, in terms of the overall objective, a companion experiment to Hard Hat and Pile Driver, a simulated surface burst in the NTS Area 15 granite seemed logical for both the experimental objectives and the logistics.

And so was born Tiny Tot.

### 1.1 OBJECTIVES

The basic reason for Tiny Tot was to furnish data needed for the design of hardened underground structures such as command centers and launch control facilities. If such facilities were to be built, estimates would be needed of the threat against which they should be hardened. These estimates included the probability of megaton surface or near-surface bursts. The results of the Hard Hat and Pile Driver programs are instructive as to the design of the structures themselves; they show that structures can be designed to withstand ground motion of about 20 ft/sec (1 kilobar in granite), but it was still necessary to know the depth to which kilobar shocks might extend. Since Tiny Tot was conceived, it has become as important to know about strong shocks near the surface and to know how the strength of direct shocks compares to motions induced by air blast.

Therefore, the first specific purpose of Tiny Tot was to produce data with which to normalize empirical extrapolation and theoretical (computational) prediction of ground shocks from surface bursts on hard rock. Second, Tiny Tot was to provide data on the cratering capability of nuclear explosions in hard dry rock, an extremely different medium from the alluvium in which most

[REDACTED]

previous nuclear cratering tests had taken place.

In addition, Tiny Tot was the first underground cratering shot, and the phenomena in the cavity and the test instrumentation itself were of interest. The stemming of shots fired in cavities is more difficult than for closely tamped shots. Planning and preparation were then underway for the Red Hot and Deep Well shots of Ferris Wheel, and it was hoped their similar instrumentation could be improved with the benefit of Tiny Tot experience.

## 1.2 TEST CONFIGURATION

When Tiny Tot was still to be fired on a ground-level surface, it was to have had a 500-ton yield and programs for measuring ground shock, crater dimensions, crater ejecta, air blast, and both prompt and residual radiation. Going underground required compromises. No imaginable cavity would be large enough for measurements of fallout or crater ejecta. It was believed the ground shock and cratering objectives could be met with a cavity that could be built, provided the yield was reduced. The choice of a [REDACTED] yield was based on the availability of a proven device of the smallest acceptable yield, though it was recognized that upgrading the frequency response of the then-available instrumentation systems would be required (Figure 1.1).

Granite was the medium chosen for Tiny Tot because of its availability at NTS, its previous use in Hard Hat (and planned use in Pile Driver), and its projected use for the underground structures of concern.

The Tiny Tot cavity was a hemisphere of 35-foot (10-meter) radius, distorted prolately along an axis normal to the flat surface so that air shocks would not focus back on the shot point. The flat

[REDACTED]

surface was 16 degrees from vertical, with the shot point at its center.

The size of the Tiny Tot cavity was chosen to give a flat surface with a radius roughly [REDACTED] times the predicted crater radius, to give reverberation times long enough to separate direct and secondary ground shock, and to reduce forces on the wall to within the elastic range of the rock. The volume was also consistent with stemming requirements.

The flat surface was made nearly vertical to shorten roof spans, making the cavity more stable and easier to build (and less expensive), and to allow the crater ejecta to fall clear of the crater. The postshot cavity was expected to be, and was, heavily contaminated with radioactive material; having the crater already empty would decrease the time required to survey it. A vertical face also meant that ground motion instrument holes could be at the same level as the cavity; no elevator from cavity to instrument drift was required. The exact slope of the face was chosen to coincide with the natural joint planes so it would be as smooth as possible.

The depth of the cavity, leaving 300 feet of rock between its top and the surface, was a conservative choice based on stemming considerations.

In its final configuration, then, the Tiny Tot excavations consisted of a shaft 387 feet deep, a main drift 200 feet long, and an instrumentation drift in a quarter circle of 100-foot radius, and of course the cavity itself. Various instrument holes were drilled between the cavity to the instrument drift or alcoves. Details of these will be given later.

[REDACTED]

### 1.3 EXPERIMENT PLAN

Tiny Tot was fired on June 17, 1965, at 1000 hours PDST (1700Z).

The yield of the Tiny Tot device was not determined directly but inferred from previous firings of the same device. In response to a request for yield determination, the answer was, "It seems to me most unlikely that these requirements can be met. The geometry of the emplacement precludes the determination of yield by hydrodynamic methods, and makes the problem of obtaining an acceptable radiochemical sample very difficult. It is highly probable, in my opinion, that the yield of Tiny Tot will never be known better than  $\pm 20$  percent; it is quite likely that even this uncertainty cannot be achieved, and that it will be necessary for DASA to use the yield values of the [device] determined from previous firings" (Reference 12). [REDACTED]

As executed, Tiny Tot had the seven projects listed in Table 1.1. At one point in the planning there had also been a Project 2.1, Fireball Measurements, to be fielded by EG&G. It was to have been a rehearsal of methods planned for Red Hot and Deep Well but, because the proposed project was quite expensive and did not have a direct use on Tiny Tot (not being precise enough for yield determination), it was canceled. Project 9.11 was added in January 1965 to give data on the magnitude of transient cable currents and electromagnetic fields generated by the explosion and their effect on instrumentation. Its report was cancelled at the direction of Headquarters, DASA, in mid-1966.

The remaining six projects included one on airblast measurements in the limited space of the cavity, four on ground-shock

DNA  
(6)(3)  
(4)(1)

[REDACTED]

measurements, and one on the true crater and other reentry observations. In addition, there have been extensive calculations of the Tiny Tot ground shock—to be discussed in Chapter 3—and there were seismic measurements made by others, welcome but not part of the DASA program.

The overall schedule of Tiny Tot is given in Table 1.2, from the time Ferris Wheel itself was conceived to the time the shot was finally announced, a time span of almost four years.

TABLE 1.1 LIST OF TINY TOT PROJECTS

Project Number	Project Title	Agency	Project Officer	Results in Reference
1.1	Cavity air-pressure measurements	BRL	J. H. Keefer	1
1.2	Ground-motion measurements	SRI	C. T. Vincent	2
1.3a	Ground high-pressure measurements	SRI	C. T. Vincent	2
1.3b	Ground high-pressure measurements	ITRI	P. Lieberman	3
1.4	Close-in stress/time	SC	H. M. Miller	4
1.9	Reentry investigations (including crater)	SC	I. D. Hamilton	5
9.11	EMP support measurements	ITRI	J. E. Bridges	Report canceled

TABLE 1.2 TIME SCALE, TINY TOT

	Reference
Ferris Wheel conceived	Jan. 62
Ferris Wheel formalized	Mar. 62 6
B-series canceled	13 May 63
Sauer and Brode push A-2	14 May 63 8
A-2 concept	6 June 63
Test Ban Treaty signed	Aug. 63
Advisory Panel decides to go underground	5 Sept. 63
First Tiny Tot concept	27 Feb. 64 10
Authority to go ahead	9 Apr. 64
Renamed Tiny Tot	28 Apr. 64
Project Officer's Planning Meeting	20 May 64
Drilling at Disappointment Hill	June 64
Drilling at final site	July 64
Contractors chosen	15 July 64
Shaft started down	27 Aug. 64
Shaft complete, drift started	27 Oct. 64
Cavity started	2 Jan. 65
Cavity complete	20 Apr. 65
User occupancy	13 May 65
OK'd by Test Evaluation Panel	18 May 65
Final FPF	11 June 65
Shot fired	17 June 65
Public Announcement	22 Sept. 65

*Page 19 is  
deleted*



## CHAPTER 2

### GROUND SHOCK

There were four projects measuring ground shock on Tiny Tot: 1. 2, 1. 3a and b, and 1. 4; their results are reported in References 2, 3, and 4. This chapter summarizes what they did, how and why, and compares the results with other relevant shots, especially Hard Hat, Shoal, Pile Driver, and Flat Top I. The next chapter takes up the related calculations and how they help to make sense out of the Tiny Tot results.

#### 2.1 INSTRUMENTATION

When Ferris Wheel was conceived in early 1962, DASA had already recognized that the conventional instrumentation of ground shock needed to be supplemented. The usual instrumentation consisted of accelerometers, velocity meters, and strain gages. These gages are valuable in the region of their validity, but they are limited at higher stresses by their mechanical strength and that of their signal cables. Aside from time-of-arrival measurements and a few peak-stress measurements (Reference 13), no data existed in the region of hydrodynamic ground shock, yet it was in this high-stress region that ground-shock phenomena are the simplest theoretically and that theoretical calculations must start. For that reason DASA had been subsidizing the development of the necessary gages for a number of years.

The new gages were piezoresistive. One kind, developed by the Illinois Institute of Technology Research Institute (IITRI),

[REDACTED]

relies on the decrease of resistance of water, paraffin, or carbon tetrachloride with increase of pressure. In a cylinder containing the piezoresistive material two platinum probes are maintained at a fixed voltage difference, and any pressure-caused change in the resistance of the material between the probes establishes a measurable change in electric current.

The gage developed by the Stanford Research Institute (SRI) relies on the increase in resistance of manganin with pressure. A gage consists of a length of fine manganin wire placed transverse to the direction of shock propagation and connected to appropriate electrodes. With a constant current applied to the wire, increase in ambient stress causes a measurable increase in voltage across the wire.

The use of these gages in Tiny Tot was the business of Projects 1. 3a and b. Both gages had seen extensive use in the Flat Top series of HE shots fired in 1964 (Reference 7). As a result of the Flat Top experience, the recording and triggering systems for these gages were changed. Each gage's signal was recorded three ways, on a single-sweep oscilloscope, on a continuously interleaved raster scope, and on magnetic tape. Triggers for the single-sweep scopes were located 6 inches closer to the zero point than the gages, but in use every single-sweep scope triggered on the zero time transient.

Project 1. 4 provided time-of-arrival measurements with Slifer cables and pressure measurements with quartz gages. Slifer cables are cables furnishing the inductive part of the resonant circuit of an oscillator. As a cable is crushed by an advancing shock front, the frequency of its oscillator changes.

Project 1. 2 provided classical measurements with accelerometers, velocity gages, and strain gages. It also had some

[REDACTED]

miscellaneous and monitoring functions, such as motion of the surface 300 feet above the cavity. The velocity gages used were Crescent Model 101258 for high-range measurements and CEC Model 4-160H for low-range measurements. The accelerometers used were Endevco Corporation and Wiancko models and an SRI-built diaphragm gage acting on the variable reluctance principle. Strain gages were SRI-built, also acting on the variable reluctance principle.

Project 1.2 recording was on magnetic tape. Twenty-six of the gages (all of the diaphragm accelerometers and all of the strain gages) were mediated by a so-called FMX system, employing a direct frequency-modulation output of the input earth motion (Reference 2, p. 68). There was no data output from the FMX system. The other gages (all velocity meters and 17 accelerometers) used the Wiancko 3 kHz carrier system and did yield data.

## 2.2 EXPERIMENT DESIGN

Holes for the gages for Projects 1.2, 1.3, and 1.4 were drilled at various angles from the working point to intersect the instrument drift.

There were five main holes as Table 2.1 shows.

Hole 0 can be used to illustrate how the first four holes of Table 2.1 were used. Nearest the device were nine piezoresistive gages of Projects 1.3a and b, four from SRI, and five from IITRI. These were at 2 to 6.9 feet and were expected to cover a range of stresses from [REDACTED] each gage having a dynamic range factor of 4. Behind these were the gages of Project 1.2—six accelerometers, six velocity meters, and four

[REDACTED]

strain gages. These were at distances of 11 to 70 feet and were intended to cover a range of [REDACTED] each gage having a dynamic range factor of 8.

Hole 1 differed from Hole 0 principally in that, to cover all bets, gage ranges were higher. The exact number of gages also differed. Hole 2 had no piezoresistive gages in it, only Project 1.2 gages. Hole 3 differed in that it had FMX accelerometers and no velocity meters.

Hole U5, used by Project 1.4, had two 33-meter and one 4.6-meter Slifer cables and two quartz gages at 51 and 79 feet. Because gage orientation problems were not as important here as for the other projects, this hole did not start at the working point but about 1/2-foot away.

Flat Top I results had been plagued by questions about gages poorly matched to the surrounding rock. In Tiny Tot, the high-stress piezoresistive gages of Projects 1.3a and b were made of granite insofar as possible. The manganin wires of the SRI piezoresistive gages were glued directly to granite cores. The IITRI piezoresistive cups were inclusions in granite blocks. The whole assemblage of granite blocks and cores was packaged in an abrasion shield of 1/8-inch steel, making a cannister 80 inches long and 6 inches in diameter.

Holes 0, 1, 2, and 3 were all drilled from the working point. They had to intersect there because the closest gages were only 2 feet from the center of the device, and the gages needed to point directly at it. Three of these four holes were 8-inch holes which, combined with overbreak, meant quite a pit in the face where the device was to be installed (Figure 2.1a). Therefore, after the gage strings were installed, carefully positioned (Figure 2.1b) and grouted in place (Figure 2.1c), granite

[REDACTED]

cylinders were placed over them (Figure 2. 1d). A shoe-shaped granite keystone was then grouted in place and the face contoured to receive the Tiny Tot device (Figure 2. 1e). Figure 2. 1f shows a device mockup in place with the apex of the plumbbob at the working point.

The grout used to fill the interstices near the device was a magnetite-loaded grout designed to match the density and sonic velocity of the granite. Its shock properties have been determined (Reference 20, Table VIII) and are compared in Figure 2. 2 with those of the granite.

### 2. 3 CAVITY CONDITION

The nuclear device was half buried in the flat face of the Tiny Tot cavity (Figure 2. 3). The 16-degree slope had been chosen to go along the natural joint structure of the rock in the hope of getting the smoothest possible face. In the chapter on cratering there is a contour map of the face (Figure 4. 1) showing deviations from planarity of  $\pm 0. 5$  foot within 10 feet of the working point and  $\pm 1$  foot within 20 feet. The region above and to the right of the shot was the roughest, the joint plane appearing to give out in that direction. Because of poor light, no photograph shows this very well; Figure 2. 4 is the best available.

In the construction of the cavity, safety required that the whole inside surface be covered with net and rock-bolted. Both of these features show in Figure 2. 4 and more plainly in Figure 2. 5. The region just around the working point is shown in Figure 2. 6 at a stage between Figures 2. 1c and 2. 1d. The rock bolts on the face were 16 feet long and in rectangular array with a spacing of 6 feet. No rock bolts were within 4 feet of the working point. The net was chain link fencing, mesh opening 2 inches,



[REDACTED]

relate them in this report data have been freely interconverted using the Hugoniot data of Figure 2. 2. (However, in the calculational results discussed in the next chapter the Hugoniot of the equation of state assumed in the calculations should be, and is, used.)

Below [REDACTED] this data relation is almost a straight line with a slope of [REDACTED]. Using that conversion, the Tiny Tot results have been plotted as radial stress in Figure 2. 8 and as peak particle velocity in Figure 2. 9. Similar data from Hard Hat, Shoal, and Pile Driver—shots of larger yield fully contained in granite—have been scaled [REDACTED] and plotted here also. Two lines are drawn through the contained data. The upper one is from a calculation by Physics International which will be discussed in Section 3. 2. The lower one is an "eyeball fit."

DNA  
(b) (3)  
(u) (1)

Scatter about the lower curve is roughly a factor of two either way, though the data from any one of the three contained shots is more narrowly confined. This curve appears to be a good overall fit to the data from previous shots in granite, and it will be used as a reference to compare with the Tiny Tot data.

Tiny Tot data were taken in holes at various angles to the normal, Hole 3 being at the extreme of 60 degrees, or only 30 degrees from the flat surface. There is a definite tendency for the high-stress data from Hole 3 to be lower than for Holes 0 or 1 but no comparable tendency for separation between data from Holes 0 and 1. The quartz-gage datum is anomalous. Empirically, both arrival-time and peak-motion data imply a nearly spherical front with very little dependence on angle except perhaps for extreme angles.

On the other hand, practically all the Tiny Tot data lie below the contained shot data, implying a definite decoupling of the shot

[REDACTED]

[REDACTED]

due to its initial position on a free surface. This was expected. Indeed the effectiveness of a surface burst as compared to a contained burst is the most sought-after single factor relative to ground motion beneath a nuclear surface burst. It is a comparison of stress or velocity/distance curves from surface bursts with those from contained bursts of the same yield, quantitatively defined as the [REDACTED] of ratio of on-axis distances to the same peak stress or velocity:

[REDACTED]

The surface burst effectiveness is not expected to be constant throughout the entire range of magnitude of ground motion and furthermore depends upon the energy coupled to the ground during the early stages of the detonation.

For the Tiny Tot configuration—a large mass-to-yield configuration [REDACTED] competent unweathered granite—the surface burst effectiveness appears to be between [REDACTED] for stress levels of [REDACTED] obar and peak velocity levels of [REDACTED]/sec, levels of interest to designers of underground protective structures.

2.4.3 Results, Precursors and Other Thoughts. Hugoniot tests on Area 15 granite show a two-wave structure for peak stresses below [REDACTED] kilobars, a precursor of about [REDACTED] kilobars followed by a plastic wave. This two-wave region shows in Figure 2.2b as a region of constant shock velocity.

These properties of granite combined with the stress decay of Figure 2.8 suggest that a two-wave structure should be evident in the Tiny Tot records taken between 2-1/2 and 5 feet from the

[REDACTED]

center of the device, and that the separation of elastic and plastic waves should increase from [REDACTED] in this region. Of the 12 high-stress gages that gave data, 10 were in this range of distances. Three of these ten were SRI gages, and seven were IITRI gages (PK and PL, respectively in Table 2.4). All of the SRI gages show apparent precursors; the IITRI gages do not.

The three precursor levels reported from SRI gages are plotted in Figure 2.10 together with the 12 peak stresses that were measured. Their wave shapes are shown in Figure 2.11. They are too few to make other than casual observations: They are of about the expected magnitude and they seem to decrease in strength with distance. The wave shapes indicate that at Station 102 ( $r = 2.54$  feet) the elastic and plastic waves are just beginning to separate, and at Stations 103 and 302 ( $r = 2.93$  feet) the two waves are fully distinct.

About the precursors, two further questions remain: Why didn't the IITRI gages observe them, and what is it that appears to be a precursor on velocity gage 207UR (Reference 2, p. 96)? Dr. Lieberman, the IITRI project officer, simply says, "the separation of the elastic and plastic wave fronts was not resolved" (Reference 3, p. 115). Five of the nine IITRI waveforms, from Gages 003, 103, 104, 301, and 303, show initial detail that Lieberman attributed to the gages being mismatched with their surroundings (Reference 3, p. 62). These double jumps are listed in Table 2.4. Their waveforms are shown in Figure 2.12. The double jump is quite pronounced for Gage 103. We might hypothesize that the first step is a precursor; however, the [REDACTED] kilobar step shown in the record is much stronger than a precursor in granite ought to be. We can imagine reasons for a precursor being less strong than the one measured in Hugoniot experi-

[REDACTED]

ments but none for [REDACTED] and [REDACTED] kilobar precursors. Indeed, the double steps are all in ratios of [REDACTED] of the peak, suggesting a systematic feature of the gage or of its installation.

The precursor reported on velocity Gage 207UR (Reference 2, p. 96; see also Figure 3.13 of this report) is at a level of [REDACTED] kilobars. An argument that might be made against the waveform of Gage 207UR being interpreted as a precursor waveform is that the gage was too far out. Sauer defends the reasonableness of calling it a precursor by pointing to some theoretical work by Alverson (Reference 31). Alverson treated spherical shocks in an elasto-plastic medium with strain hardening. He found that in such a medium, once the precursor is well formed and separated from the following main shock, it will continue its independent existence, attenuating separately from the main shock, including within the so-called elastic region below the yield point. Another puzzling point is that if a precursor is evident at the 13-foot range of Gage 207UR it ought also to be evident at the 16-foot range of Gage 208UR and on the more distant gages. In the waveform from 208UR (Figure 3.14) no broad plateau is to be seen, only a hesitation about halfway to the first peak. Similar hesitations are evident on the waveform of Gages 209UR and 009UR. Seven other velocity gages do not show any such step, but all 11 gages have about the same rise time to peak pressure: [REDACTED] second. Rise times so slow are themselves worthy of notice although they have been observed before, in this medium and others. Long rise times in the so-called elastic range have never been satisfactorily explained. Finally, the possibility suggested by the calculations reported in the next chapter that the 207UR precursor is the remains of an air-shock-induced ground response only evident at this, the shallowest

[REDACTED]  
velocity gage in Hole 2. The record is real. Results are too few to resolve the source of the precursor.

## 2.5 INSTRUMENT PERFORMANCE

As mentioned before, there were a number of experimental gage systems used in Tiny Tot. After the fact, we can look back and see how well they worked. A tabular summary is given in Table 2.7. None of the FMX systems worked; apparently the zero-time transient cable currents knocked out the FMX oscillators, and they did not recover until after signal arrival (Reference 2, p. 82). Other gages too suffered from these transients. (It is noteworthy that the most successful set of velocity gages was that in the 45-degree Hole 2 where there was no high-stress canister and hence less intimate coupling with the shot). In general, velocity gages did well, with some trouble due to early crushing of the canisters. All accelerations were higher than expected, with the result that most instruments were overranged. On the other hand those accelerometers on the surface 300 feet over the cavity almost all worked well.

As to the IITRI and SRI high-stress gages, the record is quite happy. Of 22 installed, 15 were apparently still good at shot time, and 12 of these gave some useful data—peaks in each case, and time histories in some cases. The resulting data, Table 2.4, make it clear that the backup recording on raster scopes and tapes was very much needed.

## 2.6 EMPIRICAL SUMMARY

The effective shock velocity in the linear region is [REDACTED]  
[REDACTED] in agreement with laboratory measurements.

The effective coupling factor from this surface burst in the

[REDACTED]

region of interest to designers of underground protective structures was [REDACTED] percent.

The data by themselves are insufficient to demonstrate nadir angle effects. (In Chapter 3, this conclusion is modified.)

Precursors were observed on three of the ten gages within the proper range of distances. The other seven gages apparently did not have the resolution required to observe precursors. One velocity gage showed an apparent precursor. Other gages in the same line merely showed long rise times.

[REDACTED]

TABLE 2.1 INDEX OF MAIN GAGE HOLES

Hole Number	Alternate Hole Designation*	Angle with Normal	Project Which Used
0	U1	0°	1.2 and 1.3
1	U2	30°	1.2 and 1.3
2	U3	45°	1.2
3	U4	60°	1.2 and 1.3
U5		15°	1.4

\*Used by the driller and occasionally in Reference 3.

TABLE 2.2 VELOCITY AND DISPLACEMENT DATA

Gage Number	Range	Angle	Arrival Time	Peak Velocity	Precursor Velocity	Peak Displacement
	feet	deg	msec	ft/sec	ft/sec	inch
007	11	0	[REDACTED]	[REDACTED]	[REDACTED]	[REDACTED]
008	14	0	[REDACTED]	[REDACTED]	[REDACTED]	[REDACTED]
009	19	0	[REDACTED]	[REDACTED]	[REDACTED]	[REDACTED]
010	30	0	[REDACTED]	[REDACTED]	[REDACTED]	[REDACTED]
011	45	0	[REDACTED]	[REDACTED]	[REDACTED]	[REDACTED]
013	70	0	[REDACTED]	[REDACTED]	[REDACTED]	[REDACTED]
107	11	30	[REDACTED]	[REDACTED]	[REDACTED]	[REDACTED]
108	14	30	[REDACTED]	[REDACTED]	[REDACTED]	[REDACTED]
109	19	30	[REDACTED]	[REDACTED]	[REDACTED]	[REDACTED]
110	30	30	[REDACTED]	[REDACTED]	[REDACTED]	[REDACTED]
111	45	30	[REDACTED]	[REDACTED]	[REDACTED]	[REDACTED]
207	13	45	[REDACTED]	[REDACTED]	[REDACTED]	[REDACTED]
208	16	45	[REDACTED]	[REDACTED]	[REDACTED]	[REDACTED]
209	21	45	[REDACTED]	[REDACTED]	[REDACTED]	[REDACTED]
210	32	45	[REDACTED]	[REDACTED]	[REDACTED]	[REDACTED]
211*	43	45	[REDACTED]	[REDACTED]	[REDACTED]	[REDACTED]
211	47	45	[REDACTED]	[REDACTED]	[REDACTED]	[REDACTED]

Source: Reference 2, Table 3.2 and Figures 3.1, 3.2, and 3.4.

\*Velocity gage oriented normal to the working face.

(THIS PAGE IS UNCLASSIFIED)

TABLE 2.3 ACCELERATION DATA

Gage	Range	Angle	Arrival Time	Peak Acceleration	Acceleration from Velocity Gages
	feet	deg	msec	g	g
007	11	0	[REDACTED]	[REDACTED]	[REDACTED]
008	14	0	[REDACTED]	[REDACTED]	[REDACTED]
009	19	0	[REDACTED]	[REDACTED]	[REDACTED]
010	30	0	[REDACTED]	[REDACTED]	[REDACTED]
011	45	0	[REDACTED]	[REDACTED]	[REDACTED]
013	70	0	[REDACTED]	[REDACTED]	[REDACTED]
107	11	30	[REDACTED]	[REDACTED]	[REDACTED]
108	14	30	[REDACTED]	[REDACTED]	[REDACTED]
109	19	30	[REDACTED]	[REDACTED]	[REDACTED]
110	30	30	[REDACTED]	[REDACTED]	[REDACTED]
111	45	30	[REDACTED]	[REDACTED]	[REDACTED]
113	70	30	[REDACTED]	[REDACTED]	[REDACTED]
207	13	45	[REDACTED]	[REDACTED]	[REDACTED]
208	16	45	[REDACTED]	[REDACTED]	[REDACTED]
209	21	45	[REDACTED]	[REDACTED]	[REDACTED]
210	32	45	[REDACTED]	[REDACTED]	[REDACTED]
211	47	45	[REDACTED]	[REDACTED]	[REDACTED]
213	70	45	[REDACTED]	[REDACTED]	[REDACTED]

Source: Reference 2, Table 3.3 and Figures 3.5, 3.6.

TABLE 2.4 HIGH STRESS DATA

Gage	Range	Angle	Arrival Time			Peak Stress*			Precursor	Stress-time History
			SS	R	T	SS	R	T		
	feet	deg								
002 PL	2.78	0								Yes
003 PL	3.66	0								No
004 PL	4.28	0								No
102 PK	2.54	30								Yes
102 PL	2.58	30								Yes
103 PL	3.41	30								Yes
103 PK	3.44	30								Yes
104 PL	4.03	30								No
301 PL	2.05	60								No
302 PK	2.93	60								Yes
303 PL	3.5	60								Yes
305 PL	6	60								Yes

DNA  
(b)(3)  
(L)(1)

Sources: PL (IITRI) gages: Reference 3, Tables 3.2-3.4  
 PK (SRI) gages: Reference 2, Table 3.6 and Figures 3.11, 3.12

\*Two entries for peak stress on PL gages mean a double structure which the project officer attributed to the mismatch between gage and surrounding material.  
 SS - single-sweep oscilloscope R - raster oscilloscope T - tape

TABLE 2.5 SLIFER CABLE AND QUARTZ GAGE DATA

Range	Angle	Arrival Time	Peak Pressure
feet	deg	msec	kilobars
5.8	15		
7.6	15		
9.3	15		
11.1	15		
12.9	15		
Q-1 51	15		

Source: Reference 4

TABLE 2.6 DATA FROM OTHER SHOTS IN GRANITE

	Range		Arrival Time	Peak Velocity	Peak Stress
	ft or m	msec	ft/sec	kilobar	
Hard Mat: (5 kt)	4.85 m				
	5.51 m				
	306 ft				
	396 ft				
	505 ft				
	604 ft				
	784 ft				
	1000 ft				
Shoal: (12.5 kt)	1500 ft				
	1500 ft				
	5.84 m				
	7.09 m				
	8.36 m				
	23.79 m				
	35.63 m				
	303 m				
Shoal: (12.5 kt) (cont)	500 m				
	831 m				
	1301 m				
	1939 m				
	1924 m				
	1953 m				
Pile Driver: (60 kt)	813 m				
	917 m				
	1022 m				
	92 m				
	140 m				
	200 m				
	1543 ft				
	832 ft				
833 ft					
868 ft					
473 ft					
386 ft					
318 ft					

DNA  
(1)  
(2)(3)

Sources: References 13, p. 24; 14, p. 46; 15, p. 28  
 Shoal: References 16, p. 34; 17, pp. 18, 20  
 Pile Driver: References 18, 19  
 \* Velocity from integration of acceleration

[REDACTED]

TABLE 2.7 INSTRUMENT PERFORMANCE

Gage Position and Type	Installed	Number Operating at Shot Time	Results		
			Peaks	Dubious	No Good
<b>Near Working Point:</b>					
High stress - SRI	9	4	3	0	1
High stress - ITRI	13	11	9	0	2
Velocity	17	16	10	2	4
Acceleration - PZT	17	16	2	9	5
Acceleration - FMX	10	9	0	0	9
Strain - FMX	11	9	0	0	9
<b>Surface and Tunnel:</b>					
Velocity	5	5	0	5	0
Acceleration - FMX	5	3	0	0	3
Acceleration - Wiancko	10	10	8	0	2

[REDACTED]

Pages 37, 38, and 39-47  
are deleted. (b)(3)  
(A)(1)



## CHAPTER 3

### CALCULATIONS

The configuration of the Tiny Tot experiment was calculated by the Physics International Company (PI) (References 21, 22). Explicit calculations of ground motion require the use of a code capable of solving the partial differential equations for conservation of mass, momentum, and energy, subject to the boundary conditions of the configuration of the particular problem at hand. Calculations also need the constitutive relations of the rock and of the explosive used.

The classical surface-burst ground-motion problem is that of Brode and Bjork who used a Particle-in-Cell (PIC) code to calculate a megaton surface burst on tuff, with the tuff described by a hydrodynamic equation of state (Reference 23). The classical contained-burst problem is that of Nuckolls, who used a Lagrangian code to calculate the 1.7-kiloton Rainier shot in tuff, with the tuff being described as first all hydrodynamic and then wholly elastic (Reference 24). Various others have followed, particularly calculations of contained bursts in various media. In the Ferris Wheel program, PI had also calculated the two Flat Top configurations and one Air Vent burst, with advancing degrees of sophistication (References 25, 26).

The main part of the Tiny Tot calculations was carried out on PI's ELK code, a two-dimensional, coupled Eulerian-Lagrangian, plastic-elastic code specifically designed for cratering calculations. The phrase "two dimensional" means that ELK

[REDACTED]

simplifies such problems to two dimensions by taking advantage of their cylindrical symmetry. The phrase "coupled Eulerian-Lagrangian" means that ELK combines a close-in Eulerian grid (zones fixed in space past which material moves) with a Lagrangian grid (zones which move with the material) farther out. The Eulerian grid in the Tiny Tot calculation extended to a distance of about 1 meter and was used to avoid problems of zone distortion due to the violent flow; this portion used a hydrodynamic equation of state (with no stress deviators). The Lagrangian portion permitted the use of an elastic-plastic equation of state needed for the later stages of shock propagation farther out. (The earlier Air Vent/ Flat Top calculations had been made with a pure Lagrangian code, PIPE.)

### (L) 3.1 GRANITE EQUATION OF STATE

The equation of state used for the Lagrangian part of the problem is cast in the Tillotson form (Reference 27):

[REDACTED]

where  $P$  is the mean stress (pressure),

$V$  is the specific volume relative to the initial state ( $\rho_0/\rho$ ),

$E$  is the internal energy per original volume ( $\rho_0 E_m$ ), and

$A, a, b, E_0$  are constants.

The yield criterion used was a combined von Mises, Mohr-Coulomb yield, linear with the mean stress up to an upper limit:

$$Y \leq \min(Y_0, Y_1 + Y_2 P).$$

Constants used in the Tiny Tot calculations are given in Table 3.1, together with a few other pertinent factors.

[REDACTED]

Figure 3.1 shows the Hugoniot implied by this equation of state, plotted as stress versus volume. It shows clearly a discontinuity in slope at a stress of [REDACTED] kilobars. This break is occasioned by the twofold nature of the yield criterion, being the point where the linear increase of yield strength ( $Y_1 + Y_2 P$ ) reaches its limit ( $Y_0$ ). Thus it is not, strictly speaking, a Hugoniot elastic limit but a change from one kind of yielding to another. (There is actually a [REDACTED] kilobar elastic wave ahead which is never clearly distinguishable in calculated results because of the finite size of the zones.) A two-shock region (the dashed line) obtains between [REDACTED] and [REDACTED] kilobar peak stress.

The agreement, or lack of it, between Hugoniot data and this fit is shown in the shock-velocity/particle-velocity plane in Figure 3.2. This figure shows that the velocity of the precursor is overestimated, that at high stresses shock velocity is underestimated, and that the extent of the two-shock region is underestimated. The latter two points are not germane, since the 1-meter Eulerian grid used extended out to the [REDACTED] kilobar stress level.

The shock front is normally at the appropriate yield point, with maximum permitted deviation between radial stress and mean stress. Behind the front the material relaxes primarily by relieving the stress deviators, so that a small change in density behind the front implies a large change in radial stress.

The Eulerian grid used a pure hydrodynamic equation of state, which is to say no account was taken of stress deviators. It was expressed by the same constants in a Tillotson form as the form just described. It is shown in Figure 3.1 as the curve marked "hydrodynamic." The hydrodynamic equation of state allows only a one-shock structure along the Hugoniot. It underestimates shock velocities so that arrival times in the calcula-

[REDACTED]

tions cannot be expected to agree with measurement.

It should perhaps be noted that the original Tillotson formulation was set up for metal-impact problems and contained a separate description of the vapor phase of the metal (Reference 27). That part was not used in Tiny Tot, whence the entries  $\alpha = \beta = 0$  and  $E_s = V_s = \infty$  in Table 2.1.

### 3.2 CALCULATION FOR A CONTAINED BURST

Before proceeding to the two-dimensional calculation of Tiny Tot itself, the equation of state was tested by performing one-dimensional spherically symmetric calculations of a 1-kiloton explosion in granite using a related one-dimensional Lagrangian code, POD. It was these test calculations that led PI not to use the vapor-phase portion of the Tillotson equation of state. Peak stresses and particle velocities from the final test calculation are plotted with data from contained bursts in Figures 2.8 and 2.9. At short ranges the agreement is quite good. At longer ranges, the calculation is high relative to the data by as much as a factor of two.

### 3.3 CALCULATIONAL RESULTS, PEAKS

The calculation was started as a one-dimensional calculation of the source and transferred to the Eulerian grid. The calculation remained a Eulerian problem out to [REDACTED], which it reached at [REDACTED] sec with a peak stress of [REDACTED] kilobars on the axis, and after which it became a coupled Eulerian-Lagrangian problem. At [REDACTED]  $\mu$ sec the central Eulerian part was discarded as contributing nothing further to the problem; at this time the peak stress was [REDACTED] kilobars on the axis at a distance of [REDACTED] meter. The remaining pure Lagrangian problem was carried out to [REDACTED]  $\mu$ sec,

[REDACTED]  
at which time the direct ground shock was at [REDACTED] with a peak stress of [REDACTED] kilobars on the axis. The calculation required 15 hours on a Control Data 3600 computer.

Calculated peak values of stress and pressure on the axis of symmetry are plotted in Figure 3.3 together with stress data from Table 2.4. In the Eulerian calculation within [REDACTED] there is no difference between stress and pressure, but beyond [REDACTED] they differ by a significant factor since large stress deviations are allowed.

Calculated peak radial velocity along the axis is plotted in Figure 3.4 together with data from Table 2.2.

Calculated times of peaks are plotted logarithmically in Figure 3.5, both for direct ground shock and for the air-pressure pulse above the surface, together with data from Tables 2.2 and 2.4.

Angular as well as radial dependence of peak stress is shown by the contours of Figure 3.6 for the close-in region. This figure indicates the positions at which measurements of peak stress were made successfully; the numbers are the peak stresses recorded at those positions.

Angular and radial dependence of peak velocity is shown by the contours of Figure 3.7. Again, the numbered symbols represent actual measurements from Table 2.2.

Finally the beginning of crater formation is shown in Figure 3.8, where velocity vectors at the end of the calculation [REDACTED] are plotted. These vectors are plotted with respect to the Lagrangian grid in its initial configuration; actually points initially at a radius of [REDACTED] had by then been displaced radially an average of [REDACTED].

Various waveforms have been plotted, but these and their

[REDACTED]

comparison with measurement will be postponed to the next section.

Much more detail and a more comprehensive picture of what went on in Tiny Tot seems to be available in these calculations than in the actual measurements themselves. For instance, the Tiny Tot experiment concentrated on the shock wave coupled into the body of the rock rather than the surface wave, under the impression that the finite size of the cavity would render surface phenomena less meaningful and, mistakenly, that these surface motions were of less concern. The data themselves do not permit drawing contours such as are shown in Figures 3.6 and 3.7, both because the data are too few to be definitive and because they scatter too much to make nadir angle dependences evident.

[REDACTED]

At the same time as these and related calculations were being carried out, Cooper of the Air Force Weapons Laboratory was investigating the accuracy to be expected, by comparing calculated results with the theoretical in instances where an analytical solution could be obtained and by comparing the results of several different calculational methods (Reference 28). His conclusion was and is that the numerics of such problems are reproducible to within a factor of 2.

[REDACTED]

[REDACTED]

These calculations are definitely within a factor of 2 of the data. Calculated peak stresses as shown in Figures 3.3 and 3.6 appear to be above that data by an average factor of 1.5. Calculated peak radial velocities as shown in Figures 3.4 and 3.7 are above the data by an average factor of 1.6 except at the larger ranges where some data are high. The calculation is quite good, especially when we remember that it followed a narrow pulse propagated a distance many times its initial width and attenuated four orders of magnitude.

Of particular interest is the apparent coupling factor of this surface burst, defined as in Section 2.4.2 as the cube of the ratio of on-axis distances to a specified stress or velocity, compared to a contained burst of the same yield. The data imply a coupling factor of [REDACTED] percent at a stress level of [REDACTED] kilobar. Tiny Tot calculations compared with the contained calculation of Section 3.2 imply a coupling factor of [REDACTED] percent at [REDACTED] kilobars and [REDACTED] percent at [REDACTED] kilobars [REDACTED]

Barring the region near the surface where air-pressure-induced ground shock is greater than direct ground shock, Figures 3.6 and 3.7 show that the effect of the presence of the surface is to decrease the strength of the shock at off-axis points. This effect is of course stronger the farther one is from the origin; velocities at ranges shown in Figure 3.7 are more affected than the stresses shown in Figure 3.6. In the velocity range of general interest [REDACTED] Cooper has tried to fit these contours with the expression

[REDACTED]

He uses arguments along the line of ray optics (i. e., no cross-

[REDACTED]

feed) to justify the form of the empiricism (Reference 29). This turns out to be a fairly good fit, as Figure 3.9 indicates.

### 3.4 CALCULATIONAL RESULTS, WAVEFORMS

If calculated peak values agree within a factor of 2 with the data, how well does the rest of the calculated detail agree? And in particular, how do wave shapes agree?

The data are themselves imperfect in that records are often confused by crosstalk from other stations in the same hole or by zero-time transients. Comparison is also made difficult by the fact that most of the high-stress gages were nearer the working point than the 1 meter at which the Lagrangian part of the calculation started, and it is in only the Lagrangian part that detailed print-outs of calculated waves are available. Despite these qualifications, there are seven useful comparisons for evaluating the calculations against the data.

Three high-stress gages installed at ranges greater than 1 meter gave stress-time histories—103PK, 303PL, and 305PL. The cleanest waveforms from velocity gages were on the Hole 2 line, and four of these were within the 10 meters to which the calculation was carried out—207, 208, 209, and 210. The positions of all seven were near positions at which calculated results were printed out, as detailed in Table 3.2. The actual waveform comparisons are shown in Figures 3.10 through 3.16.

The Gage 103PK record is among the more interesting in that it is one of the three high-stress gages that showed precursors (Figure 3.10). The original waveform—taken on a gage with microsecond resolution—shows the precursor to be [REDACTED] wide. This precursor is not evident in the calculations. One can not hope to see a precursor this short because the use of von

[REDACTED]

Neumann viscosity to handle sharp shocks smears them out over several zones. In the Tiny Tot calculation the shortest zones were 7.5-cm long, and at a shock velocity of [REDACTED] a shock takes [REDACTED] to cross such a zone. The two calculated waveforms plotted at 1.2 meters (both shown in Figure 3.10) have rise times of [REDACTED] implying a smear of the shock over four to five zones—a not unusual number.

Another reason that the calculation will not show precursor detail at 1.2 meters is that this position is just 20 cm from the inside edge of the Lagrangian problem where the precursor is permitted to start. Figure 3.2 shows that the equation of state used implies a precursor of velocity [REDACTED] followed by a main shock of velocity decreasing from [REDACTED]. The differential is very small and implies a precursor separation on the order of 1  $\mu$ sec, unresolvable in the calculation.

The other two high-stress data shown (Figures 3.11, 3.12) were from IITRI gages which, as installed, either did not have the resolution necessary to show a precursor or were smeared out in gage mismatches. Again the calculations would not be expected to show the precursor, nor do they.

In other respects, agreement is ambiguous. No record lasts long enough to do much more than get through the peak. The one that lasts longest (103PK) does imply a decrease in stress behind the front somewhat like that calculated.

We would perhaps note the very long rise time shown in the calculated waveform of Figure 3.12. It is due to an air-induced ground shock, peaking at about [REDACTED] which arrived ahead of the direct ground shock, peaking at [REDACTED]. Of course it is not obvious in this one waveform that this is so. The plotted waveform is the radial velocity put together from its vertical and hor-

[REDACTED]

horizontal components. The air-induced shock is quite evident in the vertical component, hardly noticeable in the horizontal component. The effect is more noticeable nearer the surface.

In addition to the three high-stress gages, four velocity gages were at proper ranges and of adequate quality for useful comparisons with the calculations. In Figures 3.13 to 3.16, data on the 45-degree line are compared with calculations on the axis and 60 degrees from the axis, i. e., 15 degrees nearer the surface than the data. For Gage 207UR there was also available the calculation at 45 degrees, so this too is plotted in Figure 3.13. (The reader is warned that, in Figures 3.13 through 3.16, discrepancies in arrival times between the calculation and data were so great that the data as plotted have been moved forward [REDACTED]

The closest of these gages (207UR) is the one in whose wave shape Sauer believed he saw the same precursor just noted in record 103PK. Sauer defended this interpretation as possible and reasonable by pointing to Alverson's analysis of a shock in an elasto-plastic medium with strain hardening (Reference 31), unlike the equation of state used in the Tiny Tot calculations. What is the proper description of Tiny Tot granite would be a proper question to ask of the data. Unfortunately the data do not say much. As noted in Section 2.4.3, the data do not conform to Alverson's hypothesis in that they lack continuity with later waveforms. The data also do not conform (as Sauer points out in oral arguments) with the idea of the regime beyond [REDACTED] kilobars being wholly elastic, since again the wave fronts should show a systematic similarity. The equation of state used in PI's Tiny Tot calculations is inelastic in the region beyond [REDACTED] kilobars, but what it implies cannot be told from the calculations because the zoning is too coarse to permit a precursor to show up in the results.



Another effect does turn up in the calculated results which is interesting to try against the real world of data: the air-induced ground shock first marginally noted in Figure 3. 12. PI's calculation was carried out with an earnest attempt to put a realistic air pressure on the upper surface of the ground, Brode's analytical fit being used (Reference 23). Along the surface the time of arrival of the air shock is earlier than that of the direct ground shock (Figure 3. 5), and only at points 45 degrees down from the surface is the air-induced wave delayed enough that they both arrive at about the same time, according to the calculations.

Thus in Figure 3. 13 the very first arrival is calculated to be earlier the closer the point is to the surface; but only at 60 degrees, closest to the surface, is there a distinguishable separate air-pressure-induced wave ahead of the main wave. At 45 degrees any effect of the air-induced shock is merged with the main wave, though it is possible the slightly earlier peak velocity is due to it. In the data record from Gage 207UR, also shown in Figure 3. 13, there is the possible precursor referred to earlier. Is it possible that what we see here is a combination of precursor and air-induced wave? The data do not speak clearly.

The subsequent portions of the calculations in all four cases are below the velocity-gage data. This probably means that the equation of state used in the Tiny Tot calculation implies release adiabats that are too fast, too strong, and depart too greatly from the loading curve.

### 3. 5 CALCULATIONAL RESULTS, SURFACE MOTION

Thus far we have discussed features of the calculations which have at least a slight chance of being checked against the data. But the calculations also imply things beyond the data,

[REDACTED]

principally surface effects and effects at positions where, even if there had been gages, there would have been noticeable perturbations from the edges of the cavity. These surface motions have since aroused greater interest than they did at the time Tiny Tot was planned.

Two-dimensional contours of the times of first peaks are shown in Figure 3. 17. Near the axis the direct shock is the first arrival; indeed the air-induced shock cannot be distinguished within its wake. Near the surface the air-induced shock is the first arrival; in these instances both shocks are clearly distinguishable in the calculations. Ground velocity induced by the air shock is downward, attenuating with depth. Velocity from the direct shock is outward and upward at about 45 degrees close-in and approaches being radial farther out. At the surface the magnitude of the direct-shock velocity is greater than that induced by the air shock at all distances greater than 2 meters. The displacement due to the air shock is everywhere much smaller than displacement due to the direct shock because the time duration of the air pressure pulse is much shorter than the duration of the direct pulse.

These things can be seen more easily by examples. We include in Figures 3. 18 through 3. 21 waveforms at three angles ( $\theta = 0, 10, \text{ and } 30$  degrees below the surface) and at four distances ( $r = 3, 5, 7, \text{ and } 10$  meters). These figures show velocity components in directions natural to cylindrical coordinates—vertical and horizontal radial. (Figures 3. 10 through 3. 13 show the truly radial vector sum.) At the surface for distances out to 7 meters the air shock produces a narrow downward pulse which decays nearly to zero before the direct shock arrives. Radial response to the air pressure above is very small. Beyond 7 meters the picture changes. At about that range the air shock

[REDACTED]

becomes transeismic, which is to say its velocity becomes less than the longitudinal velocity in the ground, and an outrunning shock takes off ahead of the air shock. All curves are qualitatively different at 10 meters.

At 10 degrees below the surface the air-induced shock arrives  $r$ , is weaker, and has an appreciable outward component. At 30 degrees below the surface the air-induced ground shock arrives just before the direct shock. At 45 degrees, as we noted before, the two shocks are hardly distinguishable, and there is left only perturbation of arrival time and time of peak.

At the surface, direct shock at 3 meters (Figure 3. 18) is equally outward and upward. At 10 degrees below the surface it is also outward and upward, but at 30 degrees below the surface its direction is 22 degrees downward, evidence that at that depth the motion is only slightly affected by the free surface. As radius increases, the direct-shock velocity at the surface changes from 45 degrees upward to nearly radial, but at the greater depths effects are qualitatively similar to what they were at 3 meters. At 30 degrees below the surface, the presence of the free surface hardly influences the direct shock.

### 3.6 CALCULATIONAL RESULTS, EXTRAPOLATIONS

It is important to say what these calculational results are not, as well as what they are, lest they be extrapolated beyond their applicability. Tiny Tot permitted various checks of a calculation against reality. Peak stresses and velocities agreed within a factor of less than 2 where comparisons were possible, the calculation generally [REDACTED] Wave form errors were in the opposite direction, for the calculations were below the data behind the wave fronts. No comparison was possible to

[REDACTED]

check the calculated surface effects, although they do seem reasonable. The calculation was not carried far enough to predict any crater phenomena. Nevertheless it is our conclusion that the various comparisons which are possible do lend general credence to the results of today's calculational methods.

If one tries to extrapolate the Tiny Tot ground-motion data, one quickly runs into possibly serious errors. Current interest is in large surface bursts in rock, [REDACTED]

DNA  
(6) (3)  
(4) (1)

DNA  
(6) (3)  
(4) (1)

[REDACTED]

In the second place the primary mechanism for depositing energy into the ground for modern large-yield weapons is by radiation transport, whereas Tiny Tot's coupling was principally mechanical. In the third place, [REDACTED] whereas a "contact burst" is a surface-touching burst. A megaton contact burst is, in terms of relative scale, quite close to the ground so that this is a minor factor. In the fourth place, on the same megaton scale of distances, rock is less competent and more layered than the rock was under Tiny Tot.

To extrapolate Tiny Tot is a matter of transferring more general considerations: the calculational method; the general phenomena; the equivalent coupling factor (related however to initial energy deposition, not to total yield). Extrapolation of the data themselves is valid only into the low kiloton range of yields.

It happens that PI has used the same methods as were used to calculate Tiny Tot, modified for radiation's role in initial coupling, in the calculation of a 1.5-megaton surface burst (Reference 30). The initial coupling was [REDACTED] the air shock was the same; direct ground shock was weaker.

[REDACTED]

Thus near the surface in Tiny Tot the direct-induced upward motion [REDACTED] as the air-induced downward ground motion but not so in the [REDACTED] (Figure 3.22). That calculation, however, is not the business of this report.

### 3.7 SUMMARY OF THE GROUND-MOTION EXPERIMENT AS CLARIFIED BY THE CALCULATION

The Tiny Tot calculation was verified to better than a factor of 2 so far as peak stresses and velocities are concerned.

The calculation yielded waveforms too short to match the data; stresses and velocity were [REDACTED] the data behind the wave front. This is apparently a fault of the implications of the equation of state about relaxation adiabats. The material is too [REDACTED] behind the front.

The calculation implies angular dependences in general agreement with the data. Therefore, the surface effects implied are probably qualitatively correct.

The calculation implies an effective coupling factor of [REDACTED] percent.

The zoning of the calculation was not fine enough to demonstrate the experimentally observed precursor. This is an inherent result of coarse zoning.

Extrapolation of the data beyond the [REDACTED] kiloton [REDACTED] valid; extrapolation of the calculational methods probably is valid provided allowances are made for effects not observed at Tiny Tot's [REDACTED] yield, e. g. [REDACTED]

**TABLE 3.1 GRANITE EQUATION OF STATE**

Gross features

Density	$\rho_0 = 2.65 \text{ gm/cm}^3$
Bulk modulus	$k = 0.53 \text{ Mb}$
Shear modulus	$\mu = 0.318 \text{ Mb}$
Poisson's ratio	$\nu = 0.25$
Longitudinal velocity	$c = 0.6 \text{ cm/sec}$
Tensile strength	$0.0003 \text{ Mb}$

Constants for Tillotson E. O. S.

$A = k = 0.53 \text{ Mb}$	$a = 0$
$B = 0$	$\beta = 0$
$a = 0.5$	$E_s = -$
$b = 1$	$V_s = -$
$E_0 = 0.05 \text{ Mb} \cdot \text{cm}^3/\text{gm} = 0.1325 \text{ Mb} \cdot \text{cm}^3/\text{cm}^3$	

Yield factors

$Y_0 =$  [redacted]  
 $Y_1 =$  [redacted]  
 $Y_2 =$  [redacted]

Tillotson E. O. S. used in form:

$$P = A \left( \frac{1}{V} - 1 \right) + B \left( \frac{1}{V} - 1 \right)^2 + \left( a + \frac{b}{1 + \frac{EV^2}{E_0}} \right) \frac{E}{V}$$

Yield condition

$$Y \leq \min (Y_0, Y_1 + Y_2 P)$$

**TABLE 3.2 POSITIONS OF WAVEFORM COMPARISONS**

Gage	Data Range		Angle	Calculation		Figure
				Range	Angles	
	feet	meter	deg	meter	deg	
103PK	3.1	(1.04)	30	1.19	5, 60	3.10
303PL	3.5	(1.06)	60	1.19	60	3.11
305PL	6	(1.82)	60	2.00	60	3.12
207UR	13	(4)	45	4.02	5, 47, 62	3.13
208UR	16	(4.9)	45	5.01	5, 62	3.14
209UR	21	(6.4)	45	7.13	5, 62	3.15
210UR	32	(9.7)	45	10.13	5, 62	3.16

*Page 64-70  
are deleted*

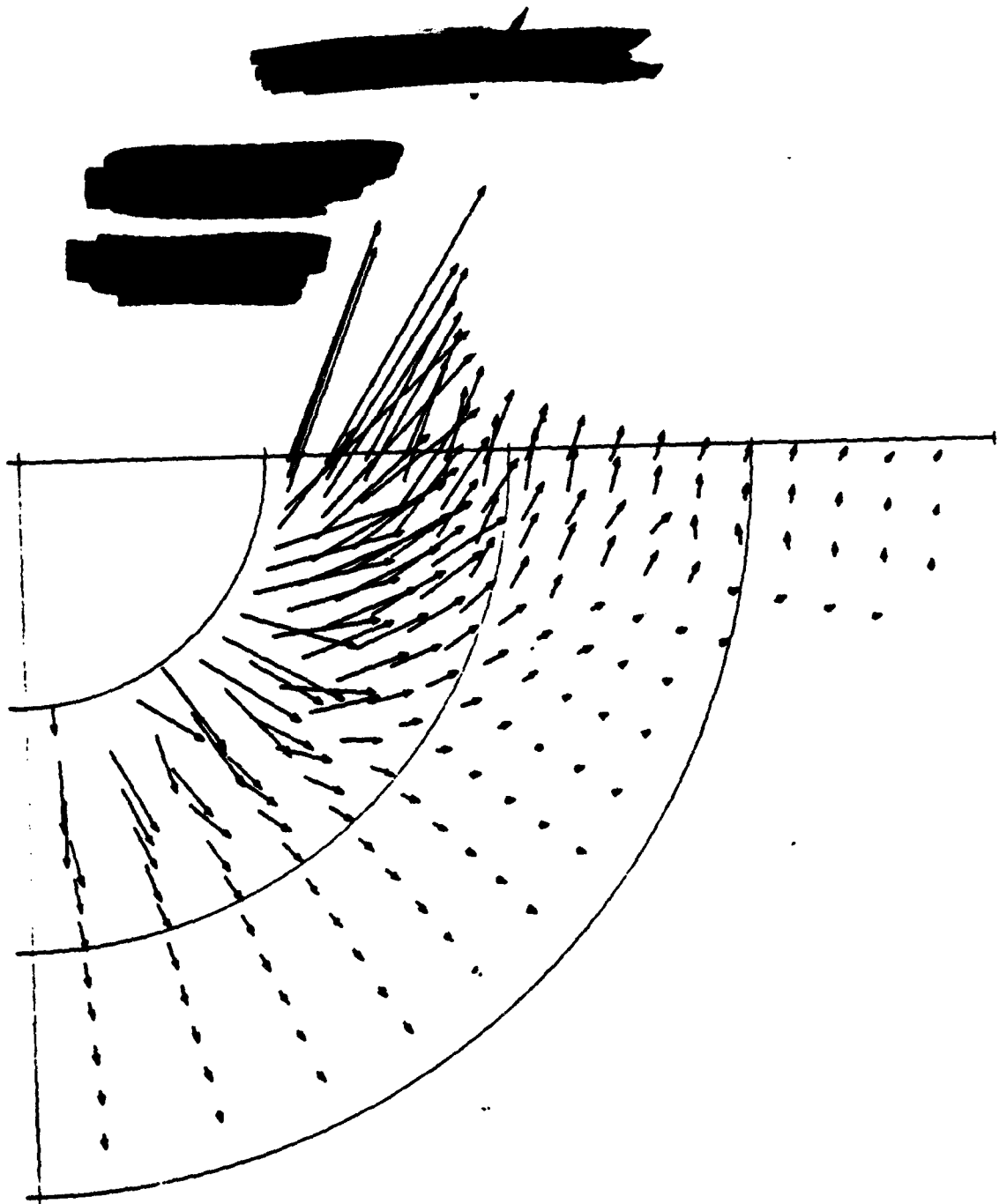


Figure 3.8 Velocity field at the end of the calculation (1790  $\mu\text{sec}$ ).

pages 72-85  
oil deleted



## CHAPTER 4

### CRATERING

#### 4.1 INTRODUCTION

When it became necessary to take Tiny Tot underground, cratering was one of the investigations still possible. The various compromises required were made so as to prejudice crater measurements as little as possible. The size of the cavity was chosen in part so that its flat surface would be bigger than the expected crater. The flat surface was tipped up in part so that the crater would clear itself. Rock bolts needed for cavity stability and integrity were spaced as far apart on the flat surface as the mining safety experts would permit.

The experiment itself had to be kept simple. It was obvious from the start that it would be desirable to go into the cavity again after the shot, and there was bound to be a good deal of radiation in it. The amount of time spent in the cavity after the shot would have to be kept to a minimum, and the tasks to be carried out there had to be kept simple.

The study of cratering is an empirical rather than a theoretical science. Ground-shock calculations have not been carried far enough to predict the crater, except for the near-optimal depths of interest to Plowshare (Reference 32). Crater measurements are of the before-and-after kind. The objective of the Tiny Tot crater program was to measure the resulting crater and the displacements around it. It was decided to forego subsurface measurements by sand columns or their hard rock equivalent.

#### 4.2 CRATER DIMENSIONS

The dimensions of the Tiny Tot crater were determined by comparing surveys made before and after the shot. Most craters

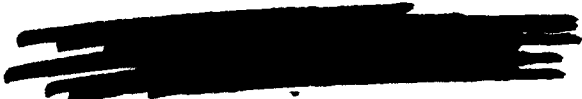
[REDACTED]

are measured by stereophotography, but this was not possible for Tiny Tot because there was not enough light and, even if there had been, cameras could not be backed off far enough from the flat face to get the necessary distortion-free field of view.

The results of the surveys are shown in Figures 4. 1 through 4. 3 as contours of preshot and postshot topography and the difference between the two, all measured relative to a plane inclined 16 degrees from the vertical (Reference 5). The result shown in Figure 4. 3 shows some bias from top to bottom which is more likely due to a slight change between preshot and postshot reference planes than to an actual residual tilt of the cavity face. Figures 4. 4 through 4. 6 show several views of the crater formed from the detonation.

True crater dimensions are tabulated in Table 4. 1 along with data from other cratering shots for the comparisons to be made in the next section. It should be noted here that we call these "true crater dimensions" because they are measured with all the loose rock removed. On a shot outdoors on a level surface some rock would have fallen back and some would not have been pushed all the way out, so that what would first meet the eye would be the so-called "apparent crater."

What first met the eye on seeing the Tiny Tot crater was a clean flat-bottomed hole in the wall that did not look very much like a crater at all. Above the hole it appeared that extra blocks had fallen away, leaving the original plane of the wall to merge abruptly and undisturbed with the freshly broken surface of the rock lining the hole. This shows in Figure 4. 3 as the protrusion upward of the minus [REDACTED] contour, in Figure 4. 5 above and to the left of the two ladders, and it is emphasized by the shadows in Figure 4. 6. Below the crater, too, blocks were broken away



but not as jaggedly as above. Those who saw the cavity and crater on first reentry report that the geometry of the pile of rock at the foot of the flat face seemed to indicate that this rubble was mostly material that had slid down rather than having earlier been flying debris. One expects to find a lip on a crater, even a true crater, because of upthrust. The appearance above and below was that any rocks displaced enough to form a lip had been separated from their fellows enough to fall away.

The clearest upthrust lip was on the right side of the crater, and there was also a low lip on the left side. In Figure 4.4, a side view, one can see the curve of the lip illuminated against a shadowed background. The rear (right) ladder is at about the slope of the original face. Figure 4.5, a front view, emphasizes the feeling of layering at the lip, as if one had bent a poorly laminated plywood until it broke.

The floor of the crater was flat as if there had been a pre-existing plane of weakness 5 feet under the original surface. This would actually be expected, since the cavity's flat surface was deliberately chosen to be a natural fracture plane and there should have been others parallel to it, especially after the stress relief upon the excavation of the cavity.

Finally there is the question of the rock bolts. How much did they affect crater dimensions? They are to be seen in all of the pictures but especially Figure 4.4.

These rock bolts were 16 feet long. They were anchored at their back end with quick-setting grout, then a faceplate was slipped over the front end and a nut was torqued tight. The residual annulus was then grouted full. Rock bolts still show in the crater. In all cases but one the plate and nut are missing. That plate (which shows most clearly in the upper left of Figure 4.4) is dished outward as if the rock had been in a hurry

[REDACTED]

to get past it. Aside from stripping of plate and nut, and some bending, the bolts show little effect of the blast. There is really no way to be sure whether these bolts did affect crater dimensions.

#### 4.3 COMPARISON WITH OTHER DATA

In Table 4.1 we also list crater data from eight other nuclear shots and from the three HE surface bursts of Flat Top. These are not all the previous data that exist—nuclear data exist for deeper bursts and for bursts at the former Pacific Proving Grounds, but they are not useful here.

The Tiny Tot data are true crater data. Most previous data are apparent crater data. In order to make valid comparisons we must either compare with the fragmentary true crater data from previous shots or make an educated guess of what the Tiny Tot apparent crater data would have been if it had been possible to fire Tiny Tot outdoors. Table 4.1 furnishes some comparisons of true and apparent crater dimensions: radii are always close to each other but depths diverge the deeper the shot. Using the shallower shots listed (Jangle S, Johnny Boy, and the three Flat Tops) we estimate that apparent crater radii and depths from surface bursts are both 14 percent less than true crater radii and depths. Thus, the estimates listed in Table 4.1 of apparent radius of [REDACTED] feet and apparent crater depth of [REDACTED] feet.

The Flat Top I shot was a 20-ton HE shot in as good rock as could be found on the surface at Nevada Test Site, a competent limestone. If one compares Tiny Tot crater dimensions with Flat Top I crater dimensions one gets an NE/HE efficiency [REDACTED] percent. This number is not very valuable, for as we said in the last chapter it cannot be extrapolated upward very far.

To compare the Tiny Tot data with any of the other data listed in Table 4.1—to obtain medium effects, for example—we

[REDACTED]

must take into account the effects of yield differences and of depth of burst (DOB). To this end the nuclear data of Table 4.1 were scaled [REDACTED] using several scalings. The resulting dimensions are plotted against DOB in Figures 4.7 and 4.8.

D & A  
(b) (3)  
(4) (1)

Figure 4.7 shows the dependence of apparent crater radius on DOB. Each circle represents [REDACTED] scaled datum from a nuclear shot in Table 4.1. The line represents the uncertainty in scaling, the outer extreme being in each case the datum scaled according to the [REDACTED] scaling in use in the Plowshare program (Reference 32a) and the inner extreme being scaled according to the [REDACTED] power of the yield, a scaling proven empirically correct for Air Vent/Flat Top HE surface-burst radii (References 7, 39, 40). The big  $\diamond$  represents Tiny Tot. Figure 4.8 is a similar curve for apparent crater depth. (The same extremes of scaling are used even though the [REDACTED] scaling was derived for radius not depth.)

In each case the Tiny Tot datum lies below the trend of the other data, an expected result. It lies at 72 percent of a straight-line interpolated radius and at 57 percent of depth. Even the larger true-crater dimensions lie beneath the other NE data. It has been postulated (Reference 41) that there ought to be discontinuity in DOB curves at the surface of the scale of the size of the device. If one interprets the previous data in this sense, as in the dashed lines, the Tiny Tot data again lie below previous data.

It is clear that Tiny Tot made a smaller crater because it was fired on sound granite. Handbook estimates are that craters in hard rock should be only 80 percent as big as craters in alluvium (Reference 42). The direction is correct, the magnitude is neither confirmed nor denied by Tiny Tot.

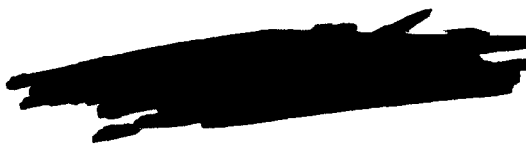
TABLE 4.1 TINY TOT AND OTHER CRATER DATA

Name	Date	Yield	DOB	Apparent Dimensions			True Dimensions			Material	Reference
				Radius	Depth	Volume	Radius	Depth	Volume		
			feet	feet	feet	feet <sup>3</sup>	feet	feet			
Tiny Tot	6/17/65								Granite	5	
Jangle S	11/19/51	1.2kt NE	-3.5	45	21	$4.45 \times 10^4$	51	21	Alluvium	33, 34	
Jangle U	11/29/51	1.2kt NE	17	130	53	$9.9 \times 10^5$	-	66	Alluvium	33	
Teapot Ess	3/23/55								Alluvium	35	
Little Feller II	7/7/62								Alluvium	36	
Johnny Boy	7/11/62	0.5kt NE	1.9	61	30.6	$1.5 \times 10^5$	67	37	Alluvium	37	
Small Boy	7/14/62								Playa	38	
Little Feller I	7/17/62								Alluvium	36	
Flat Top I	6/22/64	20T HE	0	27	12.7	10,000	38	14.5	Limestone	39	
Flat Top II	6/17/64	20T HE	0	35.8	12.9	24,000	38	16	Playa	39	
Flat Top III	3/24/64	20T HE	0	38.8	18.6	38,000	44	23	Playa	39	

\*Estimated as described in text.

\*\*The Small Boy crater was a depression crater. These numbers are the dimensions of the central part.

pages 92-99 are  
skipped



## CHAPTER 5

### AIR PRESSURES



Air-pressure measurements also remained possible when Tiny Tot was taken underground, although they were limited by the fact that the flat surface had a radius of only 35 feet. Yet this very region, the high-pressure region, was one of special interest since at that time there had been no surface measurements of direct shock over  si (in Small Boy, Reference 43) and no measurements of reflected pressure over  si. There had been photographic measurements of shock-front position from which shock overpressure could be inferred—the whole set of fireball photographs, for instance—and these had served to verify the basic theory of the fireball and the idea of how air shock starts.

Under these circumstances, air-pressure studies were incorporated in Tiny Tot as Project 1. 1, reported in Reference 1. Also, Project 1. 2 tried two air-pressure measurements in holes.

The objective of the air-pressure program was to measure airblast parameters in the very high pressure region: overpressure on the flat surface, reflected overpressure on the curved surface, free-air overpressure on a probe, and overpressure in small tubes and holes simulating tunnels.

Nine measurement stations were set up, as indicated in Table 5. 1, four at various distances on the flat surface, two on the curved surface, and three on a probe used as a baffle which extended inward from the curved surface, 60 degrees from the axis of symmetry (30 degrees from the flat). There is interest in how airblast enters tunnel openings and how it propagates down tun-

[REDACTED]

nels, so four holes were instrumented with pressure gages. Two were 3/4-inch holes near Stations 4 and 5; two were 3-inch drill holes perpendicular to the flat face.

The expected gage environment was horrendous. For instance, [REDACTED]

[REDACTED] Careful multiple shielding, stringent environmental tests, and good mechanical design of gage mounts were required. Five dummy gages were used to monitor environmental response.

Four types of gages were used. The Kaman Model K-1701-1 gage has a nonmagnetic metal diaphragm near an air-core coil. Changes in eddy current losses as the diaphragm moves cause measurable changes in gage impedance. The Dynisco Model APT 136RB gage has a diaphragm supported at its center by a thin-walled cylinder on which are bonded platinum alloy strain gages. The Schaevitz-Bytrex Model HFG gage has a diaphragm supported at its center by a column to which are bonded semiconductor strain gages. Wiancko pressure gages were used by Project 1. 2.

The results are tabulated in Table 5. 1. Only five believable records resulted. There were no successful measurements in the tunnels, for various reasons. Table 5. 1 does list a measurement in the more distant Brode hole, as reported in the Project 1. 2 preliminary report. By the time of the final report, however, Sauer had second thoughts about its validity (Reference 2, p. 82), believing instead that this apparent [REDACTED] psi signal was due to acceleration sensitivity of the gage. On the other hand, the reported arrival time of [REDACTED] msec is late compared to other acceler-

[REDACTED]

ometer arrival times (Table 2. 3) but is about what one would expect from a shock transmitted all the way through air. Figure 5. 1 indicates an arrival time of [REDACTED] msec at the entrance to this hole. A pressure of [REDACTED] psi travels at about [REDACTED] ft/sec and would take [REDACTED] msec to reach the end of the hole. Accordingly this datum has been included in Table 5. 1.

In Figure 5. 1 the actual and predicted arrival times are plotted for comparison, and Figure 5. 2 compares measured incident peak pressure with predictions. The first very obvious fact is that all three shock arrivals on the flat surface are delayed, relative to expectation and relative to those away from the flat surface. Here, then, is clear evidence of a nonsphericity of the shock front, a drag on the so-called flat surface.

Peak pressures included one measurement at [REDACTED] psi, higher than ever before measured with electronic instrumentation. That value is somewhat above what was predicted. It is one of only three direct measurements of incident pressure, since two of the successful stations were mounted directly on the curved surface and saw only a reflected pressure; the other two incident pressures are below what was predicted. It may or may not be significant that the record from Station 4 departs more from the prediction than that from Station 9; if real, it is consistent with the observation just made of surface drag effects.

Wave shapes from Stations 1, 6, and 9 are quite clean, having well-defined shock fronts and a not impossible amount of oscillation thereafter. Indeed the record from Station 9 shows distinct incident and reflected signals [REDACTED] msec apart. The record from Station 5, after baseline corrections made from the accompanying dummy environmental gage, is of the same quality. By contrast the record from Station 4 (Figure 5. 3a) is full of hash,

[REDACTED]

and incident and reflected waves are not easily distinguishable. Table 5.1 lists the reflected wave as starting a [REDACTED] msec. That choice is reasonable in that Station 4 was about 3-1/2 feet from the curved surface, and a delay of [REDACTED] msec is about the right [REDACTED]

One troubling feature of the data is the magnitude of the reflected pressures. Theoretically incident and reflected shock fronts should be related by a reflection factor

$$R = \frac{\Delta P \text{ reflected}}{\Delta P \text{ incident}} = 2 \left[ \frac{1 + \frac{3\gamma - 1}{4\gamma} Z}{1 + \frac{\gamma - 1}{2\gamma} Z} \right]$$

where  $\gamma$  is the ratio of specific heats (1.4 for air at S. T. P.) and  $Z$  is the ratio of the incident overpressure to preshock ambient air pressure. The reflection factor should be somewhere between 2 and 8 (for  $\gamma = 1.4$ ) or between 2 and 9 (for  $\gamma = 1.33$ ) and, at high incident overpressure ratios such as here, the reflection factor should be near the upper end of its possible range. Yet if we take the Station 4 and 9 data literally, we get  $R = 1.7$  and  $R = 2.6$ . If we take account of the fact that these measurements were made at 4 and 1-1/2 feet from the reflector, and that in this distance the incident pressure would decay further as implied by Figure 5.2, we can raise the apparent reflection factors to something like 2 and 3. These are also too low. Possible explanations are the irregularity of the curved surface (no effort was made to keep it smooth) and, for Station 4, surface drag effects. An explanation not possible is preheating of the surface by radiation, both because the levels are too low ( $5 \times 10^{14} \text{ n/cm}^2 \approx 20 \text{ cal/cm}^2$ , and only about 1 percent of thermal radiation has been emitted by

[REDACTED]

shock arrival time) and because measurements at Stations 5 and 6 right on the surface are well behaved.

Peaks from Stations 5 and 6 also can be used to infer reflection factors. Station 5 was nearly behind Station 4. Extrapolating the peak at Station 4 by the slope of Figure 5.2 yields an incident pressure of [REDACTED] psi at Station 5. Reading from Figure 5.2 at the range of Station 6 yields an incident pressure of [REDACTED] psi for that station. These together with the measured reflected pressures of [REDACTED] and [REDACTED] psi imply reflection factors of [REDACTED] and [REDACTED].

In connection with the detection program, Brode ran some calculations on shock waves within spherical cavities (Reference 44). These calculations imply that after reflection from a spherical wall, the pressure decreases in strength very rapidly as it runs back into the center again. Perhaps such a phenomenon is responsible for the very low reflected pressures at Stations 4 and 9.

A final point of interest from the air-pressure program: the gage at Station 4 survived a fairly long time, time for air pressure in the cavity to start to come to a long-time equilibrium. The long-time record from Station 4 is shown in Figure 5.3b. After the first few reverberations within the cavity the air pressure was about [REDACTED] psi; a [REDACTED] seconds it was about [REDACTED] psi.

TABLE 5.1 AIR PRESSURE MEASUREMENTS

Station	Range feet	Surface	Gage Type	Measurement	Arrival Time msec	Overpressure psf
1	11	Flat	Kaman	Overpressure	[REDACTED]	[REDACTED]
2	16	Flat	Kaman	Overpressure	[REDACTED]	[REDACTED]
3	20.7	Flat	Bytrex	Overpressure	[REDACTED]	[REDACTED]
4	29.5	Flat	Kaman	Overpressure	[REDACTED]	[REDACTED]
			Dynisco	Tunnel	[REDACTED]	[REDACTED]
			Dynisco	Overpressure	[REDACTED]	[REDACTED]
			Dynisco	Tunnel	[REDACTED]	[REDACTED]
			Dynisco	Reflected	[REDACTED]	[REDACTED]
			Dynisco	Overpressure	[REDACTED]	[REDACTED]
			Dynisco	(incident)	[REDACTED]	[REDACTED]
			Dynisco	(reflected)	[REDACTED]	[REDACTED]
5	33	Curve	Kaman	Reflected	[REDACTED]	[REDACTED]
			Kaman	Overpressure	[REDACTED]	[REDACTED]
			Kaman	Tunnel	[REDACTED]	[REDACTED]
6	36.7	Curve	Dynisco	Reflected	[REDACTED]	[REDACTED]
			Dynisco	Overpressure	[REDACTED]	[REDACTED]
9	30	Probe	Kaman	Overpressure	[REDACTED]	[REDACTED]
			Kaman	(incident)	[REDACTED]	[REDACTED]
			Kaman	(reflected)	[REDACTED]	[REDACTED]
10	21	Probe	Kaman	Overpressure	[REDACTED]	[REDACTED]
11	14	Probe	Kaman	Overpressure	[REDACTED]	[REDACTED]
0801-PR	10 x 40*	Flat	Wiancko	Tunnel Reflected	[REDACTED]	[REDACTED]
0802-PIL	17 x 40*	Flat	Wiancko	Tunnel Reflected	[REDACTED]	[REDACTED]

\*Hole was 10 feet from working point and 40-feet deep.

\*\*Preliminary numbers--discounted in final report, Reference 2.

*Pages 106-108  
are deleted*

[REDACTED]

## CHAPTER 6

### THE CAVITY

The new and then unique thing about Tiny Tot was that it was fired in a cavity underground. Design considerations and how they worked out are the concern of this chapter, including the special problems of containment against release of radioactivity.

#### 6.1 CAVITY DESIGN

The size of the Tiny Tot cavity was chosen to give a flat surface larger than the expected crater, to be able to separate direct and secondary ground shocks, and to be consistent with stemming requirements. The shape and orientation of the cavity were chosen for construction ease, to simplify postshot reentry, to take advantage of natural joint planes, and to simplify installation of instruments.

Clearly a flat surface was needed but it had to be finite, and a primary concern was that its very finiteness might degrade the measurements. Compromises enough had been made by going underground and eliminating measurements of fallout, ejecta, surface motion, and apparent crater. The remaining measurements of ground shock, true crater, and high air pressure were to be as representative as possible of what they would have been for a shot in the open.

Cavity dimensions were not changed after April 1961 though the arguments for those dimensions were improved later. A flat surface with a radius of [REDACTED] (meters) was [REDACTED] [REDACTED] as the expected crater and hence allowed for some upthrust

[REDACTED]

around the crater. Air shock was predicted to arrive at the cavity walls at [REDACTED] with a strength of [REDACTED] reflecting to [REDACTED] and to reverberate with a period of [REDACTED]. This allowed an interesting range of air-pressure measurements. It meant that secondary ground-shock signals from the corner would be about [REDACTED] behind direct ground shock at a distance of [REDACTED] feet into the rock and that these indirect signals would be weak. Secondary signals from reverberation would arrive [REDACTED] msec after the main signal; they were defocused by the natural roughness of the curved surface and by deliberately making it somewhat aspherical and hopefully would not significantly distort the data.

## 6.2 STEMMING DESIGN

The stemming problem was to design a system of plugs for the entry tunnels to retain the radioactivity within the cavity. These plugs had to resist the forces inside the cavity, so it was necessary to estimate the long-term as well as the transient forces.

The cavity was to have a volume of [REDACTED] and an internal area of [REDACTED]. A first estimate was made assuming no losses, all the energy [REDACTED] to remain in the air of cavity. At an elevation of 5000 feet, the density of air is about  $1 \times 10^{-3}$  gm/cm<sup>3</sup>, so that the energy density in the air after the shot would be. [REDACTED]

DNA  
(b)(3)  
(b)(1)

Such a pressure was more than the overburden pressure ( $\rho gh = 340$  psi), and the temperature was far above any reasonable equilibrium temperature, the vaporization point of the rock itself being only about 2500°C.

[REDACTED]

Such a pressure and temperature would last only momentarily, then decrease as the surrounding material started to share the temperature of the cavity. At the time of the shot, estimates were made of heat conduction into the rock of the walls of the cavity and into the surface of the crater debris, and that in itself was sufficient to cool the cavity enough in seconds that the internal pressure would be below overburden pressure —specifically, the estimates were that [REDACTED] would be carried by conduction into that rock [REDACTED]. Since then an error has been recognized in the ejecta surface area that was assumed and this loss by rock conduction is reduced [REDACTED] but it has also been recognized that the large amount of steel in the cavity [REDACTED]

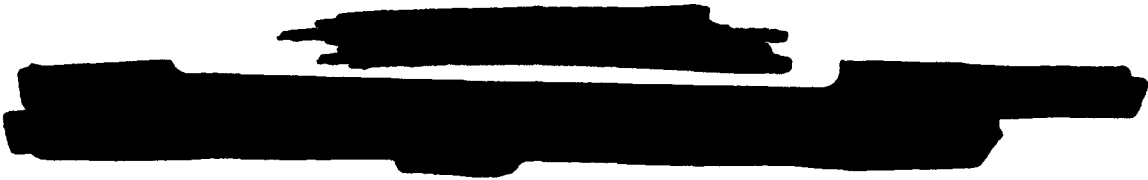
[REDACTED]  
[REDACTED] constituted a heat sink capable of absorbing a large fraction [REDACTED] energy release.

P.H.A.  
(5) (3)  
(4) (1)

[REDACTED]

[REDACTED]

[REDACTED]



### 6.3 SHOT TIME BEHAVIOR

To monitor any possible leaks, six Remote Area Monitoring System (RAMS) units were installed, as indicated in Table 6. 1. What was read by these monitors is shown in Figure 6. 1.

Radioactivity began to appear between Plugs 1 and 2 almost immediately, and levels in the neighborhood of 1000 R/hr were reached in 10 minutes. During this time there was an increase in air pressure to 5 psi that lasted several minutes. Activity penetrated more slowly past Plug 2, reaching levels of 60 to 100 R/hr in 1-1/2 hours. Activity came through the sand plug and reached levels of 100 R/hr in 3-1/2 hours. Surface levels never exceeded 1 R/hr and fluctuated wildly, apparently depending on the strength of the wind at the mouth of the shaft.

Figure 6. 1 shows a pronounced drop in the reading of RAMS Units 3, 4, and 5 at about 6 hours. This drop may be spurious. The AEC Test Manager had directed that bentonitic drilling mud be dumped into the shaft to try to control the leak. This would have covered Unit 5, and reentry later showed that the added weight broke the bulkhead below, allowing the mud to fill the space monitored by Units 3 and 4.

Final atmospheric release has been estimated at about 700 curies, measured at release time. The activity released was predominately xenon with a small contribution from iodine:  $^{138}\text{Xe}$  - 700 Ci, radioiodines - 21 Ci. About 90 percent of the release came in the first 14 hours (Reference 47).



#### 6.4 REENTRY OBSERVATIONS

Reentry was delayed by a strike at the test site (the shot date itself had been accelerated for the same reason). First reentry was a hole drilled down from the surface for TV monitoring only. The principal purpose of this was to assure that the cavity had survived with little damage.

The principal reentry in September 1965, about 3 months after the shot, was through the shaft and tunnel. The shaft was only slightly damaged. The tunnel outside Plug 2 was filled with drillers mud which had to be mucked out. Plug 2 was bypassed by mining. The instrument drift, though contaminated, was very little damaged mechanically. Plug 1 was also bypassed by mining, permitting direct entry to the cavity. There, high alpha and beta-gamma levels required double protection suiting, full masks, and supplied air.

The leaks at Plug 2 are believed to have been where cables passed through the  plug. No leaks were observed around it, but small ones there cannot be ruled out.

Leaks past Plug 1 were evident from water seeping into the drift from the cavity. Most of this was at the contact between  and granite at the top and to the side of the plug. In addition, the Project 1.1 cables to the instrument drift were somewhat permeable to gas.



#### 6.5 CONDITION OF THE CAVITY

Except for the crater in the flat face and the rubble pile at the bottom, the cavity's rock outline was altered very little by the detonation. There is now about 10 feet of sand filling the bottom of the cavity, added to reduce radiological hazards during reentry by giving a clean surface on which to walk.

[REDACTED]

When fired, the cavity was lined on all inside surfaces (except just next to the shot) by steel net held down by plates on the ends of rock bolts. Catwalks on the flat surface had been removed, but others were left on the curved surface. On reentry much of the netting was gone; all the remaining catwalks were missing, presumably lying in the rubble at the base of the cavity. Most of the plates on the rock bolts were still in place, and many were still tight against the rock.

There was no evidence of prolonged high temperatures within the cavity. A close-up of part of the curved wall is shown in Figure 6. 2. It appears that the net failed mechanically. Many strands of wire remain pulled to the left—away from the flat surface. Their ends appeared to be necked down and broken in tension but not melted. In the stub of the access drift between cavity and shaft a good deal of rubble had been jammed up against the plug.

[REDACTED]

[REDACTED]

[REDACTED]

The Project 1. 1 gage at Station 4 survived to give long-term pressures within the cavity. After the first few reverberations, the air pressure within the cavity was [REDACTED] psi as predicted; it continued to decrease on a time scale of seconds as shown in Figure 5. 3b.

## 6. 6 CONCLUSIONS

The stemming design appears to have been basically sound. Leaks around the seat of [REDACTED] plugs have also been seen or suspected on more recent shots and are apparently exceedingly difficult to prevent entirely. Thus the presence of a second plug as backup was necessary. Still, the first plug successfully with-

[REDACTED]  
stood pressures [REDACTED]  
[REDACTED]  
[REDACTED]

Leaks along the cables could have been controlled better than they were, by considering the prevention of leaks as a criterion in procurement and by potting junction boxes along them.

The cavity itself is not fit for prolonged occupation. Alpha levels in it require protection that would increase the costs of any operation there, and the loss of protective netting means any prolonged use of the cavity would involve considerable danger from rock falls.

The Pile Driver shot of June 2, 1966, damaged the Tiny Tot shaft to the point where extensive rehabilitation would be required to make it usable again.

TABLE 6.1 [REDACTED] RAMS UNIT LOCATIONS [REDACTED]

---

No. 1	At end of instrumentation drift
No. 2	In instrumentation drift near main drift
No. 3	Just on shaft side of Plug 2
No. 4	At base of shaft
No. 5	50 feet up shaft, on top of sand
No. 6	At mouth of shaft

---



## CHAPTER 7

### SURFACE AND SEISMIC MOTIONS

#### 7.1 SURFACE MOTIONS

Motions of the surface above the cavity were measured by SRI in Project 1.2 and by the U. S. Coast and Geodetic Survey (CGS) (References 2, 48). SRI's measurements were along a simple line extending roughly northwest to southeast. The CGS measurements included a circle of gage stations at a horizontal range of 165 meters (540 feet), each station containing Statham gages measuring three components of acceleration. At greater distances the CGS had NGC-21 seismometers in three components. A tabulation of some of these data is given in Tables 7.1 and 7.2.

The SRI data indicate a subsurface spall out to a range of more than 350 feet in both directions. The CGS data are beyond the spall and therefore are to be compared to SRI's first peaks. This comparison, made in Figure 7.1, gives some confidence the gages are indeed measuring the same thing.

The interesting hint from the CGS ring of stations is of strong directional effects. In Figure 7.2 are plotted maximum resultant accelerations in various directions from the shot cavity. The flat surface of the cavity, points northwest (313 degrees), and this is the direction of the greatest signal. Individual components of signal are not as regular as the resultant, and indeed individual maxima usually occur at entirely different times. The maximum vector resultant in every instance but one (Station 1) occurred with the peak positive vertical signal, even though there often was a larger negative vertical signal.



[REDACTED]

## 7.2 SEISMIC DECOUPLING

The phrase "big-hole decoupling" means that if a shot is fired in a hole big enough that the wall signal is elastic or nearly so, the teleseismic (low-frequency) signal will be reduced (Reference 49). The idea was tested and proved in Cowboy and in the Salmon and Sterling shots.

The Tiny Tot configuration, although it was big enough, did not meet the usual criteria for decoupling because the cavity was hemispheroidal, and the device was not in the center of the cavity. Nevertheless it was of interest to determine the influence of the cavity on the seismic signals at a distance (Reference 51).

Two of the stations in the Sandia seismic network around NTS had also been operated on the Hard Hat shot, fired in the same granite and very close to Tiny Tot. These were at Tonopah, Nevada (149 km, N47° 29'W) and at Darwin, Nevada (173 km, S52° 32'W). Each station is equipped with three-component, short-period (1 second) Benioff seismometers.

In Hard Hat seismic motions of [REDACTED] were recorded at Darwin and [REDACTED] at Tonopah. On Tiny Tot the two stations operated properly, but no signals were discernible above the noise. The measured noise level was taken as the upper limit of a possible Tiny Tot signal and compared to a linearly scaled Hard Hat signal. On this basis it appears that Tiny Tot was decoupled by at least a factor of [REDACTED]. A different scaling of Hard Hat signal might raise that figure.

**TABLE 7.1 PROJECT 1.2 SURFACE MOTION DATA**

Gage	Horizontal	Azimuth	Arrival	First	Maximum
	Range				
	feet	degree	msec	g	g
9003 AV	345	294	[REDACTED]	[REDACTED]	[REDACTED]
AH	1				
9002 AH	173	294			
9000 AV	8	-			
9102 AV	177	114			
9103 AV	350	114			
AH					
9104 AV	704	114			

\* Waveform of a spill signal.  
 AV - acceleration vertical  
 AH - acceleration horizontal

**TABLE 7.2 USCGS SURFACE MOTION DATA**

Station	Range	Azimuth	Peak Acceleration			
			Vertical	Radial	Tangential	Resultant
	meter	degree	g	g	g	g
1	165	42	[REDACTED]	[REDACTED]	[REDACTED]	[REDACTED]
2	165	90				
3	165	135				
4	165	180				
5	165	224				
6	165	270				
7	165	313				
8	165	0				
9	405	312	[REDACTED]	[REDACTED]	[REDACTED]	[REDACTED]
11	1034	312				

Notes: Up, away clockwise are positive  
 Peaks do not necessarily occur at same times

*Pages 121-122  
 are selected*

## REFERENCES

1. John A. Keefer; "Nuclear Airblast Phenomena in an Underground Cavity"; Tiny Tot Project 1.1, POR-3015, November 30, 1967; Ballistic Research Laboratories, Aberdeen Proving Ground, Maryland; (SRD)
2. F.M. Sauer and others; "Close-In Earth Motion Studies/Pressure Measurements in the Hydrodynamic Region"; Tiny Tot Projects 1.2/1.3a. POR-3016, December 4, 1967; Stanford Research Institute, Menlo Park, California; (CRD)
3. P. Lieberman; "Close-in Stress-Time History Measurements"; Tiny Tot Project 1.3b, POR-3017, June 19, 1968; IIT Research Institute, Chicago, Illinois; (CFRD)
4. R.C. Bass and H.M. Miller; "Close-in Shock Studies"; Tiny Tot Project 1.4, POIR-3015, June 12, 1967; Sandia Corporation, Albuquerque, New Mexico; (CFRD)
5. W.D. Weart; "Post-Shot Reentry Investigation of the Tiny Tot Drift and Cavity"; Tiny Tot Project 1.9, POR-3019, October 8, 1968; Sandia Corporation, Albuquerque, New Mexico; (CRD)
6. "Nuclear Cratering and Ground Shock Research Program"; DASA-60540, March 1962; (SRD)
7. M.L. Merritt; "Air Vent/Flat Top Summary Report"; POR-3000, September 27, 1968; Sandia Corporation, Albuquerque, New Mexico; (U)
8. H.L. Brode (Rand Corporation, letter to Chief, DASA, Attn: J.G. Lewis, L-10200, May 14, 1963; (C)
9. M.L. Merritt; "Test Concept, Ferris Wheel, Event A-2"; Sandia Corporation, Albuquerque, New Mexico; RS 5412-309, June 6, 1963; (SRD)
10. M.L. Merritt; "Test Concept, Ferris Wheel Event A-2"; Sandia Corporation, Albuquerque, New Mexico, February 27, 1963; (CFRD)
11. M.L. Merritt; "Test Concept, Ferris Wheel Event Tiny Tot (A-4)"; Sandia Corporation, Albuquerque, New Mexico, April 11, 1964; (C)
12. A.C. Graves, LASL, letter to J.E. Reeves, NVOO/AEC, Ref No. JDO-1765, October 12, 1964; (SRD)
13. R.C. Bass and A.J. Chabai; "Summary of Measurements on Spherical Shock Waves from Buried Nuclear Explosions"; SC-WD-64-559, Sandia Corporation, Albuquerque, New Mexico, April 1964; (SRD)
14. W.R. Perret; "Free Field Ground Motion Studies in Granite"; Operation Nougat, Shot Hard Hat, Project 3.3, POR-1803; April 19, 1963; Sandia Corporation, Albuquerque, New Mexico; (OUO)
15. L.M. Swift; "Measurement of Close-in Earth Motion"; Hard Hat Project 1.2, VUP-2101, March 15, 1962; (U)

[REDACTED]

16. W.D. Weart; "Free Field Earth Motion and Spalling Measurements in Granite"; Shoal Project 1.1, VUF-2001, October 18, 1965; (U)

17. R.C. Bass and others; "Hydrodynamic and Plastic Shock Studies"; Shoal Project 45.3, VUF-1003; Sandia Corporation, Albuquerque, New Mexico; (U)

18. W.R. Perret; "Free Field Motion"; Pile Driver Project 1.2a, POR-4001, September 26, 1968; Sandia Corporation, Albuquerque, New Mexico; (U)

19. R.C. Bass, Preliminary Pile Driver data

20. T.J. Flanagan; "The Hugoniot Equation of State of Materials for the Ferris Wheel Program"; Sandia Corporation, Albuquerque, New Mexico, SC-M-66-451, September 1966; (U)

21. D.J. Andrews; "Two-Dimensional Calculations of Explosions in Layered Media"; Physics International Report, PIFR-036, Vol II, March 22, 1967; (CFRD)

22. D.J. Andrews to Merritt, and others, letter enclosing preliminary results of Tiny Tot calculations, December 14, 1966.

23. H.L. Brode and R.L. Bjork; "Cratering from a Megaton Surface Burst"; Rand Corporation, RM-2600, June 30 1960.

24. W.J. Frank, ed.; "Proceedings of the Second Plowshare Symposium"; UCRL-5675, May 15, 1959; (U)

Chapter c2.: J.H. Nuckolls; "A Computer Calculation of Rainier (the First 100 Milliseconds)."

25. C.S. Godfrey and others; "Prediction Calculations for Free-Field Ground Motion"; AFWL-TDR-64-27, May 1964.

26. C.S. Godfrey and others; "Calculations of Underground and Surface Explosions"; AFWL-TR-65-211, June 1966.

27. J.H. Tillotson; "Metallic Equations of State for Hypervelocity Impact"; General Atomics, GA-3216, July 18, 1962.

28. H.F. Cooper, "Comparison Studies of Finite Difference Results for Explosions on the Surface of the Ground"; AFWL-TR-67-25, April 1967.

29. H.F. Cooper; "Free Field Motion from Surface Bursts on Rock"; AFWL-TR-67-94, August 1967; (SRD)

30. D. Maxwell and D. Andrews; "ELK-18, -A Calculation of the Free Field Response of Granite Following a Surface Burst"; Vol I-IV, P-I Interim report on contract DA-49-146-XZ-476, March 1967; (C-Limited distribution)

31. G.E. Duvall and R.C. Alverson; "Final Report - Fundamental Research in Support of Vela-Uniform"; Stanford Research Institute, Contract No. AF 49 (638)-1086, May 31, 1964.

32. a. "Engineering with Nuclear Explosions: Proceedings of the Third Plowshare Symposium"; TID-7965, p. 75-98, April 1964.

b. J.T. Cherry; "Computer Calculations of Explosion Produced Craters";

[REDACTED]

International Journal of Rock Mechanics and Mining Sciences, Vol IV, p. 1-22 (1967).

33. J.D. Bishop and F.E. Lowance; "Physical Characteristics of Crater and Lip"; Jangle Project 4.2, WT-375, August 1952; Naval Civil Engineering Research & Evaluation Lab., Port Hueneme, California; (U)

34. L.J. Vortman; "Jangle True Crater Measurements"; SC-RR-64-19, Sandia Corporation, Albuquerque, New Mexico, February 1964.

35. J.G. Lewis; "Crater Measurements"; Operation Teapot Project 1.6, WT-1105, July 1955; Engineer Research & Development Laboratory, Ft Belvoir, Virginia; (SRD)

36. A.D. Rooke and J.N. Strange; "Crater Size and Shape"; Operation Sun Beam, Shots Little Feller I and II, Project 1.9, POR-2263, March 25, 1965; Waterways Experiment Station, Vicksburg, Mississippi; (SRD)

37. A.D. Rooke; "Crater Measurements"; Operation Sun Beam, Shot Johnnie Boy, Project 1.9, POR-2284, April 9, 1965; Waterways Experiment Station, Vicksburg, Mississippi; (SFRD)

38. A.D. Rooke and others; "Crater Measurements"; Operation Sun Beam, Shot Small Boy, Project 1.9, POR-2208, March 3, 1965; Waterways Experiment Station, Vicksburg, Mississippi; (SFRD)

39. A.D. Rooke and L.K. Davis; "Crater Measurements"; Flat Top Project 1.9, POR-3006, August 9, 1966; Waterways Experiment Station, Vicksburg, Mississippi; Sandia Corporation, Albuquerque, New Mexico; (U)

40. T.J. Flanagan; "Crater Studies"; Project Air Vent, SC-RR-64-1704, Sandia Corporation, Albuquerque, New Mexico, April 1966.

41. "Ground Shock and Survival or Kill of Military Systems"; DASA-1836, October 1966; (SRD)

42. "Capabilities of Nuclear Weapons"; TM-23-200, Revised Edition, November 1964; (C-Gp3)

43. J.H. Keefer and others; "Nuclear Airblast Phenomena"; Operation Sun Beam Shot Small Boy, Project 1.1, POR-2200, December 1963; Ballistic Research Laboratories, Aberdeen, Maryland; (CFRD)

44. H.L. Brode; "Nuclear Explosions in Cavities"; RM-3727, November 1965.

45. G. Plass and others; "A Theoretical Study of the Motion of Bomb Debris"; Aeronutronic Division, Ford Motor Co., March 12, 1961; Chapter 2: Equations of State; (SRD)

46. W.D. Weart; "Tiny Tot Containment Prospectus"; an enclosure in a letter to Marshall Page (NVOO/AEC), Sandia Corporation, Division 7111, Albuquerque, New Mexico, September 1, 1964; (CFRD)

47. Memo, H.L. Rarrick (Sandia Corporation, Albuquerque, New Mexico) to Maj M.J. Colvin (FC/DASA), "Tiny Tot, U15e, Source Determination and Effluent Report, 11 + 48 Hours"; June 19, 1965; (C)

48. U.S. Coast & Geodetic Survey, unpublished data.

[REDACTED]

- 49. A. L. Latter and others; "A Method of Concealing Underground Nuclear Explosions"; Journal of Geophysical Research, Vol 66, pp. 943-946 (1961).
- 50. R. F. Herbst and others; "Use of Large Cavities to Reduce Seismic Waves from Underground Explosions"; Journal of Geophysical Research, Vol 66, p. 959-978 (1961).
- 51. D.M. Hankins; "Tiny Tot Seismic Decoupling"; SC-RR-65-381, Sandia Corporation, Albuquerque, New Mexico, August 1965; (CRD).
- 52. R.G. McQueen and others; "Hugoniot Equation of State of Twelve Rocks"; Journal of Geophysical Research, Vol 72, p. 4999-5036 (1967).

[REDACTED]

*Pages 127-130  
are deleted*

Security Classification

DOCUMENT CONTROL DATA - R & D

1. Only classification of title, body of abstract and indexing annotation must be entered when the abstract report is classified.

2. ORGANIZING AGENCY (Corporate Author)  
Defense Atomic Support Agency  
Washington, D. C. 20305

3. REPORT NUMBER  
1

4. REPORT TITLE  
Summary Report

5. DESCRIPTIVE NOTES (Type of report and inclusive dates)  
Final summary of Shot Tiny Tot accomplished on Ferris Wheel Series.

6. AUTHOR(S) (First name, middle initial, last name)  
M. L. Merritt, Scientific Director, Sandia Laboratory, Box 5800,  
Albuquerque, New Mexico 87115

7. REPORT DATE  
8. TOTAL NO. OF PAGES 132  
9. NO. OF REFS 52

10. CONTRACT OR GRANT NO.  
A. PROJECT NO.  
B. ORIGINATOR'S REPORT NUMBER:  
POR-3021  
(WT-3021)

11. OTHER REPORT NUMBERS (Any other numbers that may be assigned this report)

12. DISTRIBUTION STATEMENT In addition to security requirements which apply to this document and must be met, it may be further distributed by the holder only with specific prior approval of the Director, Defense Atomic Support Agency, Washington, D. C. 20305

13. SUPPLEMENTARY NOTES  
14. SPONSORING MILITARY ACTIVITY  
DOD/DASA

15. ABSTRACT  
Tiny Tot was a nuclear burst on the flat surface of a large underground cavity in granite. It was fired to produce data for empirical extrapolation and to normalize theoretical (computational) prediction of ground shock from surface bursts on hard rock, as well as for hard-rock crater data.  
Ground-motion experiments showed a coupling factor of [redacted]; the 1-kilo-par level. The true crater formed was [redacted] considerably smaller than it would have been in soils where most other data have been obtained. Air-pressure measurements included one [redacted] psi, the highest yet by nonphotographic methods; they also seem to show pronounced degradation of the airblast from the so-called flat surface. The stemming and containment plan was satisfactory, with only a slight leak of radioactive xenon and iodine.  
The associated calculations were verified to better than a factor of two so far as peaks are concerned, as good as could be expected. Waveforms were short in duration relative to the data, raising questions about the relaxation adiabats implied by the equation of state used.  
Extrapolation of the data beyond the low kilotons is not valid; extrapolation of calculational methods probably is valid provided allowances are made for effects not observed at Tiny Tot's low yield.

DKA  
(b)(3)  
(2)(c)





10 REV 00000	LINE A		LINE B		LINE C	
	SOLE	WT	SOLE	WT	SOLE	WT
Ferris Wheel Series						
Shot Txy Tot						
Ground motion						
Stress						
Velocity						
Precursor						
Cavity						
Crater						

